Journal of Hydrology 569 (2019) 167–187

Contents lists available at ScienceDirect

Journal of Hydrology

journal homepage: www.elsevier.com/locate/jhydrol

Research papers

Factors controlling arsenic and selected potentially toxic elements in stream sediment–soil and groundwater–surface water systems of a hydrologically modified semi-closed basin (Uluova) in Elazığ Province, Eastern Turkey

Murat Çeliker[a], Sedat Türkmen[b], Cüneyt Güler[c,*], Mehmet Ali Kurt[d]

[a] Devlet Su İşleri 9, Bölge Müdürlüğü, 23069 Elazığ, Turkey
[b] Çukurova Üniversitesi, Balcalı Kampüsü, Jeoloji Mühendisliği Bölümü, 01330 Adana, Turkey
[c] Mersin Üniversitesi, Çiftlikköy Kampüsü, Jeoloji Mühendisliği Bölümü, 33343 Mersin, Turkey
[d] Mersin Üniversitesi, Çiftlikköy Kampüsü, Çevre Mühendisliği Bölümü, 33343 Mersin, Turkey

ARTICLE INFO

This manuscript was handled by Huaming Guo, Editor-in-Chief, with the assistance of Harald Neidhardt, Associate Editor

Keywords:
Arsenic
Stream sediment
Soil
Water quality
GIS
R-mode factor analysis

ABSTRACT

The Uluova basin aquifer system (UBAS), comprised of fractured/karstic rock and multilayer basin-fill aquifers, provides water for both domestic and agricultural needs in the Elazığ province (Eastern Turkey). Although, the UBAS has been subject of large-scale hydrological modifications and controversial water management practices since late 1950s, thus far no studies have examined basinwide implications of such human perturbations in an integrated manner. In this study, GIS, geostatistics, *R*-mode factor analysis (*R*-mFA) and geochemical modeling techniques were employed to unravel the factors controlling the distribution and sources of arsenic (As) and selected potentially toxic elements (PTEs) in the stream sediment-soil and groundwater-surface water systems of the UBAS. As revealed by the results from *R*-mFA, three geogenic factors (F1: Clay minerals and Fe–Mn oxyhydroxides, F2: Weathering of parent materials, and F3: Sulfide oxidation in mineralized zones) govern the geochemical dynamics of the PTEs in the stream sediment/soil media. In stream sediment and soil samples, especially Ni, Cr, and Co presented significant enrichment relative to upper continental crust average composition, whereas As contents were relatively low, varying from 0.3 to 13 mg kg^{-1}. Factors extracted from the combined water dataset (F1: Groundwater salinization and arsenic mobilization, F2: Clay minerals and Fe–Mn oxyhydroxides, F3: pH and redox conditions, and F4: Aquifer oxygenation and nitrate contamination) accounted for 72.59% of the total variance. Water-rock interaction (e.g. sulfide oxidation, carbonate dissolution, silicate hydrolysis, adsorption-desorption, ion exchange, and evaporite dissolution), dilution/mixing with fresh/saline water components, evapoconcentration, and human induced perturbations causing internal salinization and oxygenation of the UBAS were the key mechanisms controlling the chemistry of waters and mobilization of As. In the UBAS, majority of As-rich water samples are confined to central-northern half of the basin and typically display high levels of dissolved O_2, inorganic oxyanions (HCO_3^-, SO_4^{2-} and of Si, B, Mo, Sb and V) and alkaline pH. Oxidation of sulfides (e.g. pyrite and arsenopyrite) found within the highly fractured Elazığ magmatics in the upland areas at north and subsequent competitive adsorption-desorption processes occurring under alkaline, oxidizing and high ionic strength aquifer conditions along the downgradient groundwater flow path play a pivotal role in the As-enrichment in the UBAS. As concentrations ranged between 0.02 and 367.2 μg L^{-1} in groundwater, 0.13–4842 μg L^{-1} in spring water, and 0.04–31.1 μg L^{-1} in the stream water samples, of which 20.83% exceeded the WHO provisional guideline value. In the water samples, As occurs mainly as As(V) species ($HAsO_4^{2-}$ and $H_2AsO_4^-$), indicated by the Eh-pH diagram and speciation calculations. The results of this study have shown that As enrichment in the UBAS can be attributed to both geogenic processes and anthropogenic activities that have modified the basin hydrology/hydrochemistry.

1. Introduction

In nature, arsenic (As) is widely distributed in rocks, sediments, soils, water, biota, and air (see National Research Council, 1977) and known to be a notorious health hazard to an estimated 200 million people (Bundschuh et al., 2013) in more than 70 countries worldwide,

* Corresponding author.
E-mail addresses: cuneytguler@gmail.com, cguler@mersin.edu.tr (C. Güler).

https://doi.org/10.1016/j.jhydrol.2018.11.067
Received 8 October 2018; Received in revised form 26 November 2018; Accepted 28 November 2018
Available online 11 December 2018

including Turkey (Ravenscroft et al., 2009). Arsenic is found in at least 245 different minerals as a primary constituent (National Research Council, 1977) and ranks as the 20th most abundant element in the Earth's bulk continental crust (Woolson, 1983) with an estimated average concentration of 2.5 mg kg^{-1} (Rudnick and Gao, 2014). In nature, As chiefly occurs in As(III) and As(V) oxidation states (Plant et al., 2003), prevailing over a wide range of geochemical environments (Brookins, 1988), with As(III) being 25–60 times more toxic than As(V) (Korte and Fernando, 1991). In such environments, As frequently co-exists with a number of trace elements (e.g. Ag, Al, Au, Bi, Co, Cr, Cu, Hg, Fe, Mn, Ni, Pb, Pt, Sb, Se, Sn, U, and Zn), many of which are also considered toxic to living organisms in high concentrations (Nordberg, 1998; Alloway, 2013). Human exposure to As, as well as to other potentially toxic elements (PTEs), is common through a wide variety of anthropogenic sources and activities, such as mining, mineral processing, metal smelting, manufacture of alloys, fossil fuel combustion, agrochemical production/application, wood treatment (using chromated Cu arsenate), and municipal solid waste incineration (Selene et al., 2003; Alloway, 2013). Epidemiological evidences suggest that prolonged exposure to elevated As levels, mainly through ingestion and inhalation, has potential to increase the risk of various types of cancers and other As-related diseases (Abdul et al., 2015; ATSDR, 2015). Therefore, the World Health Organization (WHO, 1993), European Economic Community (EEC, 1998), and U.S. Environmental Protection Agency (USEPA, 2009) set the limit for As in drinking water at 10 μg L^{-1}.

Since mid-1990s, in Turkey, there has been a growing interest to studies related to As contamination in different environmental media and its sources/fate in the environment. However, the As epidemic in the Turkish territory has received only a limited recognition from the international community, which can be deduced from the lack of reference to case studies from Turkey in the peer-reviewed literature (e.g. Mandal and Suzuki, 2002; Rahman, 2002; Smedley and Kinniburgh, 2002; Ratnaike, 2003; Amini et al., 2008; Zhou et al., 2017). The review of case studies found in the growing body of literature revealed that natural (geogenic) As contamination is a prevailing phenomenon, especially in western Turkey (e.g. Aegean, Marmara, and Central Anatolia regions), which mainly occurs in: (i) mineralized areas found in a wide variety of geologic and tectonic settings (Akçay et al., 1996; Karayigit et al., 2000; Çolak et al., 2003; Yılmaz, 2007; Gemici et al., 2009; Gunduz et al., 2010; Eliopoulos et al., 2012; Özkul et al., 2015; Benzer, 2017); (ii) areas of active geothermal systems (Gemici and Tarcan, 2004; Aksoy et al., 2009; Baba et al., 2009; Pasvanoğlu and Chandrasekharam, 2011; Bundschuh et al., 2013); and (iii) areas of past volcanic activity (Querol et al., 1997; Altaş et al., 2011; Yuce and Yasin, 2012; Simsek, 2013). In these studies, reported As concentrations reach up to 5900 mg kg^{-1} in stream sediments (Gemici et al., 2009) and 2488 mg kg^{-1} in soils (Özkul et al., 2015) around mineralized areas, 7754 μg L^{-1} in a cold spring (6 °C) issuing from colemanite-bearing clay zone rich in As minerals (Çolak et al., 2003), 1420 μg L^{-1} in hot fluids (137 °C) from a geothermal field (Aksoy et al., 2009), and 345 μg L^{-1} in an aquifer system developed in an area of past volcanic activity (Simsek, 2013).

Eastern Anatolia region in Turkey – hosting many important mineralized areas and polymetallic ore deposits, major active tectonic structures, geothermal fields, and a wide variety of rock/sediment types associated with the past volcanic activities – has an important potential for geogenic As contamination, which is currently understudied and poorly characterized. Nevertheless, recent studies conducted in eastern Turkey report alarming levels of As contamination, locally reaching up to 5070 μg L^{-1} in groundwater (45 °C) from Diyadin (Ağrı province) geothermal area (Pasvanoğlu, 2013) and 202 mg kg^{-1} in sediments from Geli Stream, draining a mineralized area near Baskil in Elazığ province (Kalender and Uçar, 2013). Present research builds upon a preliminary study conducted in the Uluova basin aquifer system (UBAS) (Çeliker, 2008), where reported As concentrations in one stream water and three groundwater samples exceeded (up to 29.7 μg L^{-1}) the provisional guideline value for drinking water (10 μg L^{-1}) established by WHO (1993). To date, no other studies have evaluated the As content, including other PTEs in the UBAS in an integrated manner.

In the Elazığ province with a population of 583,671 (2017 census), groundwater abstracted from the UBAS constitutes the sole source of the drinking water supply (Turkish Statistical Institute, 2018) and irrigated agriculture is the major consumer of water (Ministry of Environment and Forestry, 2014). Therefore, determination of the sources and factors controlling distribution of As and other PTEs in the environment constitutes a critical step towards protecting human health, understanding their influence on stream sediment-soil and groundwater-surface water systems, and achieving sustainable management of the soil and water resources throughout the UBAS. Complicated by the large-scale hydrological modifications and controversial water management practices over the last 60 years, the UBAS also presents a unique case study of the impact of modern human activities on the physico-chemical quality of groundwater resources. The main objectives of this study are therefore: (i) to quantify the levels of As and selected PTEs in stream sediment, soil, and water samples collected from the UBAS; (ii) to determine the spatial trends of As and selected PTE occurrences using geostatistics and GIS tools; and (iii) to identify possible sources and factors controlling the mobility of As and selected PTEs using *R*-mode factor analysis (*R*-mFA), GIS-based factor score mapping, and geochemical modeling techniques.

2. Study area

2.1. Physiographic setting, climate and land use

The Uluova basin, situated in the south of Elazığ provincial center (Eastern Anatolia region, Turkey), covers an area about 864 km^2 between the latitudes 38°23′20.67″–38°42′52.63″ N and longitudes 39°00′26.74″–39°35′38.18″ E (Fig. 1). Agricultural plain of Uluova and the part occupied by the Keban Dam reservoir together cover 46.3% of the total basin area, where the remaining portion consists of sparsely inhabited highlands that serve as recharge areas (Fig. 1). The basin itself is a complex structural and topographic depression that lies between several mountain ranges with elevations ranging from 1490 m to 2171 m above mean sea level (amsl). These mountain ranges are characterized by distinct NE-SW trends that are sub-parallel to the overall trend of the seismically active East Anatolian Fault Zone (EAFZ) (Fig. 1); capable of producing large earthquakes (Calayır et al., 2012; Çolak et al., 2012; Aktug et al., 2016).

The area has a semiarid continental climate, with a long-term (1950–2015) average annual precipitation of 410.2 mm (Turkish State Meteorological Service, 2016). Monthly precipitation in the area is highly variable between seasons (42.1% in spring, 3.8% in summer, 23.3% in fall, and 30.8% in winter) and monthly average temperatures range from −0.9 °C to 1.6 °C in winter and 22.9 °C to 27.3 °C in summer (Turkish State Meteorological Service, 2016). Due to prevailing semiarid climate conditions, evapotranspiration (ET) greatly surpasses precipitation (P) in the basin (ET/P > 1), especially during the months from June to September.

The Uluova basin is mostly rural in character where rain-fed and groundwater-irrigated agriculture dominates the land use (53.52%) in the central part and along the Haringet Stream (Fig. 2). A wide variety of crops is grown in the area, including cereal crops (barley and wheat), forage crops (corn, alfalfa, grasses, etc.), and vegetables/fruits (tomato, pepper, cucumber, onion, cantaloupe, watermelon, etc.). Numerous small-size agricultural fields (e.g. vineyards and fruit orchards) and livestock farms are also present in the area (Çetindağ and Okan, 2004). The basin floor slopes to NE with elevations decreasing from 1000 m to nearly 845 m amsl, the latter being the maximum water level of the Keban Dam reservoir (Fig. 2). Being the second largest artificial reservoir in Turkey after the Atatürk Dam, Keban Dam reservoir, with a

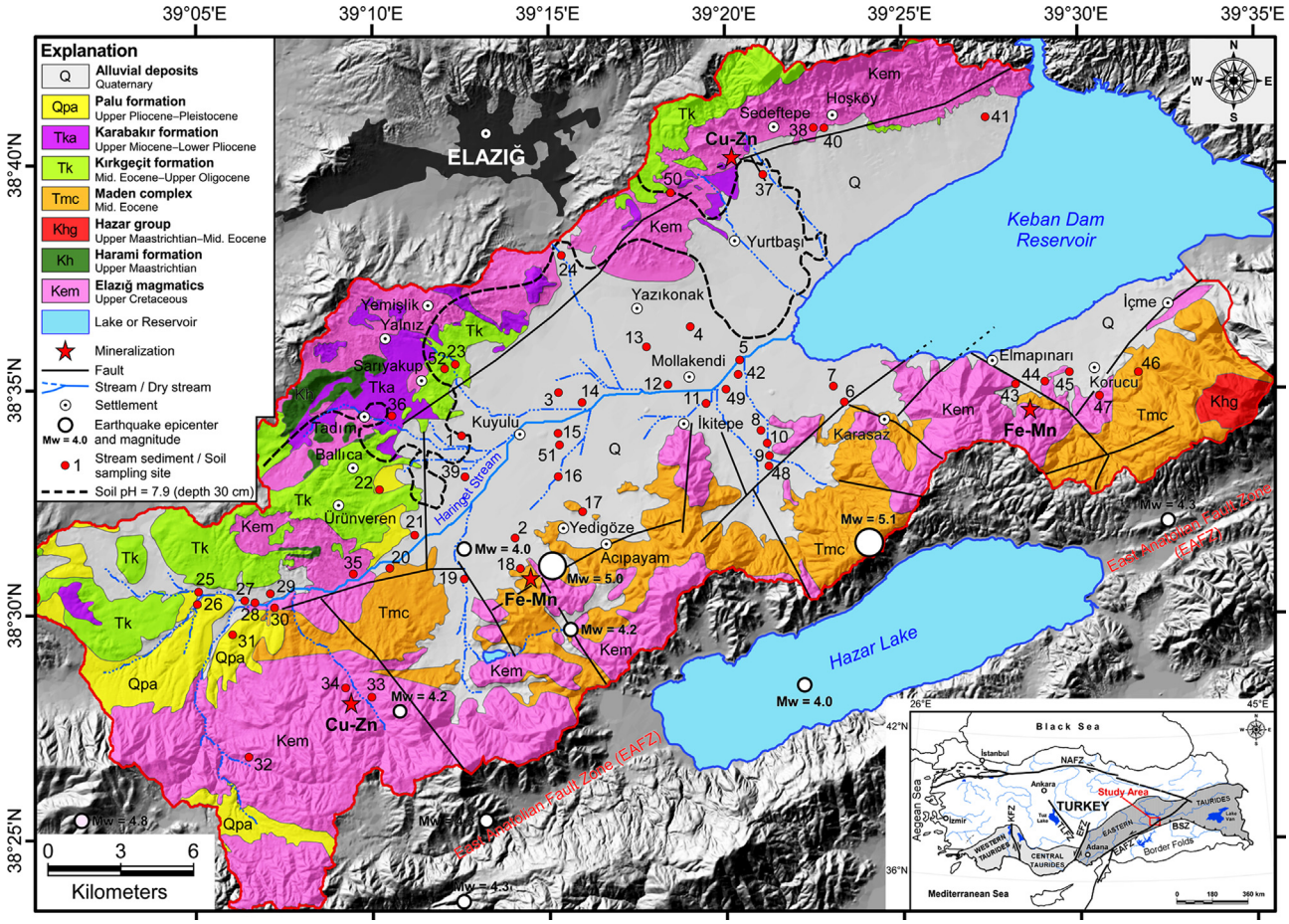

Fig. 1. Simplified geological map (adapted from Sungurlu et al., 1985; Çolak et al., 2012) of the Uluova basin, onto which stream sediment (nos. 1–28) and soil (nos. 29–52) sampling sites are superimposed. Records related to historical earthquake data retrieved from B.U. KOERI-RETMC (2017). Black heavy dashed-line represents the soil pH = 7.9, measured at a depth of 30 cm (DSİ, 2012). Inset shows the broad geographical subdivision of the Taurides (after Özgül, 1984), major tectonic features (abbreviations: BSZ = Bitlis Suture Zone, EAFZ = East Anatolian Fault Zone, NAFZ = North Anatolian Fault Zone, EFZ = Ecemiş Fault Zone, KFZ = Kırkkavak Fault Zone, TLFZ = Tuz Lake Fault Zone; modified from Jaffey and Robertson, 2005), and location of the study area (shown in red box). (For interpretation of the references to colour in this figure legend, the reader is referred to the web version of this article.)

total surface area of 675 km^2 and a length of 125 km along the Murat River Valley, reached its designed capacity in May 1976 after a construction period of almost 10 years (from 1965 to 1974). Prior to water impoundment in the Keban Dam in mid-1974, outflow from the semi-closed UBAS was toward the Murat River, of which water surface elevations ranged from 782 m to 801 m amsl (Karanjac et al., 1977). Today, nearly half of the Uluova plain, as well as vast parts of the Murat River Valley, is submerged by the Keban Dam's reservoir, which established a new constant head (at max. 845 m amsl) by laterally shifting the pre-1974 constant head westwards, significantly altering natural discharge conditions (Karanjac et al., 1977). The Hazar Lake, a tectonic lake formed within the EAFZ, is situated outside of the UBAS and some 7 km south of the Keban Dam reservoir at an altitude of ~1240 m amsl (Fig. 2). The highly saline and alkaline water (Na-Cl-HCO_3 type) of the Hazar Lake had been utilized for many decades through a 5-km tunnel system for energy production in Hazar I and Hazar II hydroelectric power plants (HEPPs) (built in 1957 and 1967, respectively) located 3.5 km apart within the Uluova basin (Fig. 2). The saline water discharged from these HEPPs, as well as freshwater from Keban Dam reservoir, had been intermittently used (at times, after mixing) between 1988 and 2006 for agricultural irrigation of the central-eastern part of the Uluova plain (covering 132 km^2) through a ~349-km-long aqueduct system built within the scope of Eyüpbağları Pumping-Irrigation Project (Çeliker, 2016). During the 1988–2006 period, the volume of water transferred to the Uluova open canal system (Fig. 2) in the irrigation season (May through October) fluctuated between 8.76×10^6 m^3 yr^{-1} and 91.5×10^6 m^3 yr^{-1} (Çeliker, 2016), with a total amount reaching 1.02×10^9 m^3. Nevertheless, a critical drop of Hazar Lake's water level (~10 m) have prompted government authorities, in January 2006, to halt operations of Hazar I and Hazar II HEPPs and to cease saline water intake from the Hazar Lake for agricultural irrigation of the Uluova plain (Çeliker, 2008). However, basinwide implications of these large-scale hydrological modifications and controversial water management practices have not been examined so far. Wastewater discharges from diverse sources and excessive use of fertilizers also put a great pressure on both surface water and groundwater resources used for supplementary irrigation (Çetindağ and Okan, 2004).

2.2. Geological setting

The Uluova basin is situated within the central part of the Eastern Taurus Orogenic Belt, which was formed along the collision zone between African-Arabian and Eurasian tectonic plates during Upper Cretaceous to Miocene period (Yılmaz et al., 1993). In the region, this collision event resulted in crustal thickening, thrust tectonism and development of complex fault systems (Sungurlu et al., 1985), such as the EAFZ (Fig. 1). The EAFZ, a NE-SW trending mega shear belt nearly 30 km wide and 700 km long (see inset in Fig. 1), consists of several faults around the study area (Aksoy et al., 2007; Çolak et al., 2012).

The geology of the basin is complex and includes Permo-Triassic

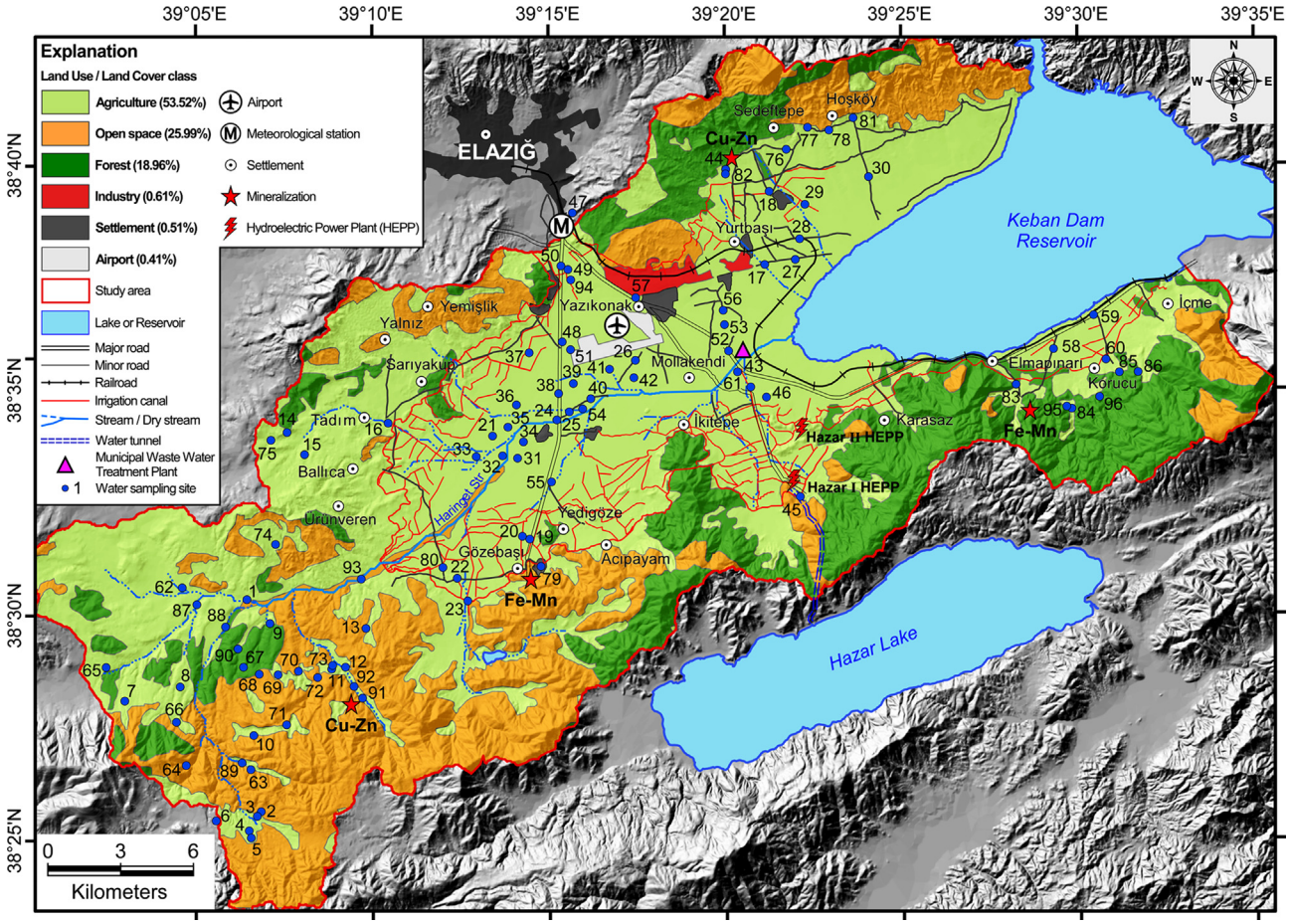

Fig 2. Map showing major land use and land cover (LULC) types of the Uluova basin (Elazığ province, eastern Turkey), onto which groundwater (n = 61, nos. 1–61), spring water (n = 25, nos. 62–86), and stream water (n = 10, nos. 87–96) sampling sites are superimposed.

metamorphic rocks, Upper Cretaceous magmatic rocks, and Cenozoic volcanic and/or sedimentary rocks (Fig. 1) formed in a variety of geologic settings. The basement is represented by Permo-Triassic Keban metamorphics that underwent greenschist-amphibolite facies metamorphism (Akgül, 1987). This unit tectonically overlies the Upper Cretaceous Elazığ magmatics (Aksoy et al., 2005; Palutoğlu and Tanyolu, 2006) and do not outcrop within the UBAS. Elazığ magmatics (a.k.a. Yüksekova complex; Perinçek, 1979) display a complex intrusive history and consist of plutonic rocks (e.g. gabbro, diabase, granodiorite, diorite, monzonite, and granite), volcanic rocks (e.g. andesite, basalt, agglomerate, and pillow lava), and subvolcanic rocks (e.g. aplite and dolerite) representing continental arc, post-collision, and within-plate magmatics (Akgül, 1993). These extremely altered magmatic rocks (Çetindağ and Okan, 2004) are unconformably overlain by Upper Maastrichtian Harami formation, composed of pelagic limestones (Sungurlu et al., 1985). In the area, Upper Maastrichtian-Middle Eocene period is represented by Hazar group, which is a well-exposed terrestrial-marine sedimentary succession consisting of detritic rocks in the lower parts and carbonate rocks in the upper parts (Aktaş and Robertson, 1984). Middle Eocene volcano-sedimentary Maden complex consists of marl, mudstone, limestone, sandstone, and basaltic-andesitic lavas (Perinçek, 1979). Middle Eocene-Upper Oligocene Kırkgeçit formation is characterized by basal conglomerates, followed upward by sandstone, limestone and marl alternations (Perinçek, 1979). Upper Miocene-Lower Pliocene Karabakır formation is composed of pyroclastic rocks, basaltic lavas, and sedimentary rocks (Sungurlu et al., 1985). In the study area, Upper Pliocene-Pleistocene Palu formation and Quaternary alluvial deposits unconformably overlie all the preceding geological formations (Çetindağ, 1985). The Palu formation can be characterized as a fluvio-lacustrine sedimentary sequence (Kerey and Türkmen, 1991) that was deposited as a result of intense tectonic activity in the region (Aksoy et al., 2007). Quaternary alluvium is characterized by poorly sorted unconsolidated materials, ranging in size from pebble to silt and clay (Sungurlu et al., 1985).

2.3. Hydrogeological setting

The UBAS is composed of fractured/karstic rock aquifers found in the mountain watersheds (i.e. recharge areas) and a multilayer aquifer system developed in the basin-fill deposits with a thickness ranging from 100 m to 350 m (Olgun and Kalkan, 1994). Confined conditions occur in the central-eastern part of the plain, as evidenced by the presence of free flowing artesian wells near the Keban Dam reservoir (Karanjac et al., 1977; Çeliker, 2008). Quaternary alluvial sediments demonstrate relatively low hydraulic conductivity values in the central part of the plain (Çeliker, 2014) due to abundance of clay-size material (Öztekin, 1998; DSİ, 2012). The general direction of groundwater flow follows the topography of the area and currently occurs towards the Keban Dam reservoir (Çetindağ and Okan, 2004; Çeliker, 2008). In the basin, recharge to the aquifers occurs both naturally and artificially through different mechanisms, such as: (i) infiltration from precipitation (rain and snowmelt), Keban Dam reservoir (after 1974), agricultural irrigation (including water transfers from the Keban Dam and Hazar Lake between 1988 and 2006), and wastewater discharges, (ii) streambed leakage, and (iii) groundwater inflow from the surrounding mountain ranges. Whereas, the discharge from the aquifers occurs through mechanisms, including: (i) evaporation of shallow groundwater, (ii) transpiration by plants, (iii) subsurface outflow to Keban

Dam reservoir, (iv) stream runoff, (v) discharge by springs, and (vi) pumping from municipal/private wells. In the 1967–1974 period, average drawdown measured in wells located in the UBAS was 6.3 m (Karanjac et al., 1977) whereas, increased groundwater abstraction to satisfy drinking and irrigation water demands resulted in a sharp decline in water levels (in average ~20 m) in the 2004–2013 period (Çeliker, 2014). The Keban Dam reservoir receives the entire surface drainage from the Uluova basin via Haringet Stream and small tributaries (Fig. 2). This ephemeral stream dries up during the summer (mean annual discharge ~1.1 $m^3 s^{-1}$) (DSİ, 2015), but a small amount of runoff occurs along the lower parts of its course due to release of municipal wastewaters and agricultural return flows (Çeliker, 2008).

3. Materials and methods

3.1. Sample collection, preparation and analyses

3.1.1. Stream sediment and soil samples

Stream sediment samples (n = 28) were collected at a depth of 0–15 cm (nos. 1–28 in Fig. 1) along the streambeds, which were mostly dry during the fieldwork. In addition, soil samples (n = 48) were collected from 24 sites at two depth intervals, i.e., 0–15 cm and 15–30 cm (nos. 29–52 in Fig. 1), which will be hereafter referred to as "upper" and "lower" soil layers, respectively. Representative stream sediment and soil composite samples (weighing ~1 kg) were obtained from randomly selected locations (Fig. 1) by pooling four subsamples (weighing ~250 g) taken on the corners of a 1-m^2 square, as suggested by Biasioli et al. (2006). The stream sediment/soil sampling and analysis procedures followed the general guidelines given by Davidson (2013). In brief, the samples were collected by a spade, then placed in self-locking polyethylene bags, labeled, and stored at 4 °C during their transfer to the laboratory. All fieldwork was completed during dry season (12–19 October 2013). In the laboratory, the samples were air-dried at ~25 °C and disaggregated in a ceramic mortar before sieving through a 2-mm nylon mesh. Finally, the fraction < 2 mm was ground finely in an agate mortar and used for chemical analyses. Chemical analyses of the samples were performed at Çukurova University (Adana, Turkey) Geological Engineering Department. A 1.0 g portion of the sample splits was analyzed for As, Co, Zn, Cr, Ni, Mn, Al, and Fe by PerkinElmer AAnalyst™ 800 atomic absorption spectrometer (AAS) (PerkinElmer, USA) after digestion in 6 mL 2:2:2 mixture of HCl:HNO_3:H_2O (*aqua regia*) at 95 °C for one hour and then diluting the resulting solution to 20 mL with ultrapure water after cooling (Candeias et al., 2014). The instrument (AAS) limits of detection were 0.2, 0.004, 0.0005, 0.003, 0.09, 0.002, 0.03, and 0.005 mg kg^{-1} for As, Co, Zn, Cr, Ni, Mn, Al, and Fe, respectively. All reagents used were of analytical grade. Prior to use, all the labware were cleaned by soaking them overnight in 5% (v/v) HNO_3 and then rinsing with ultrapure water. The QA/QC procedures employed in this study included routine analyses of blanks, duplicates, and in-house standards, bracketing every five samples.

3.1.2. Water samples

In this study, 96 water samples, encompassing groundwater (n = 61, nos. 1–61), spring water (n = 25, nos. 62–86), and stream water (n = 10, nos. 87–96) sources (Fig. 2), were collected throughout the UBAS during dry season (12–19 October 2013). Sampling and analytical techniques followed the suggestions by APHA-AWWA-WEF (2005) and were similar to those described in the literature (Güler et al., 2012). In brief, temperature, redox potential (Eh), pH, electrical conductivity (EC), and dissolved O_2 (DO) were measured on site by means of portable multi-parameter instruments (i.e. Hach HQ30d and Hanna HI 8314) under minimal atmospheric contact. Water samples were taken into two high-density polyethylene bottles (250 mL), one acidified in the field with 65% HNO_3 to pH ≤ 2 for major/trace element analyses and the other left as it is (unacidified) for anion analyses. Then, all water samples were transported to the laboratory in a cooler within 48 h and refrigerated at 4 °C until analysis. Chemical analyses of water samples were made at the Advanced Technology Education, Research and Application Center (MEİTAM), Mersin University (Mersin, Turkey). Total concentrations of five major (Ca, Mg, Na, K, and Si) and twenty trace (Al, As, B, Ba, Br, Cd, Co, Cr, Cu, Fe, Li, Mn, Mo, Ni, Pb, Sb, Sr, Ti, V, and Zn) elements were determined using Agilent 7500ce inductively coupled plasma-mass spectrometer (ICP-MS) (Agilent Technologies, Japan) equipped with Octopole Reaction System to eliminate polyatomic interferences (see May and Wiedmeyer, 1998). External standard calibration method was applied to all determinations, using an internal standard mix containing ^{6}Li, ^{45}Sc, ^{72}Ge, ^{89}Y, ^{115}In, and ^{209}Bi. Calibration curves (five-point) were constructed by analyzing NIST single-element reference standards prepared by serial dilution of stock solutions. The ultrapure water, with a resistivity of 18.2 MΩ cm at 25 °C, obtained from ELGA Purelab UHQ system (Veolia Water Solutions, UK) was used during the course of all analytical procedures. The accuracy and precision of the analytical technique was evaluated by analyzing the Certified Waste Water Trace Metals Solution (B) (High-Purity Standards, USA). Concentrations of anions (Cl^-, SO_4^{2-}, NO_3^-, HCO_3^-, and CO_3^{2-}) were determined as described previously by Güler et al. (2012). Both the relative error for individual hydrochemical parameters and calculated charge balance errors for water samples were less than ± 5%. The geochemical code PHREEQCI ver. 3.3.3 (Parkhurst and Appelo, 2015) was used to evaluate saturation states and aqueous speciation of the selected mineral phases, employing the database "llnl.dat" (Johnson et al., 2000). Mineral saturation indices (SI) with negative (SI < 0), zero (SI = 0) or positive (SI > 0) values, indicate that the water sample is undersaturated, in equilibrium or supersaturated (respectively) with the mineral phase of interest.

3.2. Data management and statistical analysis

In this study, statistical analyses were performed using R ver. 3.1.2 (R Core Team, 2014). First, descriptive statistics, histograms, and probability plots were used to examine variable distributions (i.e. normal vs. non-normal). The normality of variable distributions in the combined stream sediment-soil dataset (n = 52; samples from a depth of 0–15 cm) and combined water dataset (n = 96; 61 groundwater, 25 spring water and 10 stream water samples) were confirmed by Kolmogorov–Smirnov (K–S) test (Kolmogorov, 1933; Smirnov, 1948). Non-linear Box-Cox transformations (Box and Cox, 1964) were applied to normalize the non-normal variable distributions, stabilize the variance, and improve homoscedasticity. The one-parameter Box-Cox transformation is given as follows (Eq. (1)):

$$x_i(\lambda) = \begin{cases} \frac{x_i^{\lambda}-1}{\lambda}, & \text{for } \lambda \neq 0, \\ \log(x_i), & \text{for } \lambda = 0 \end{cases} \quad (1)$$

where; x_i is the random variable (consisting of positive and non-zero values) being transformed; i = 0,1,2,…,n − 1; and λ is the transformation parameter (Box and Cox, 1964). Data variables satisfying the normality requirement were standardized to z-scores, following Güler et al. (2002). Through standardization, the variables can be re-scaled to a range of about −3 to +3 standard deviations, thus each variable contributes equal weight in the multivariate statistical analyses (Güler et al., 2010). Both the combined stream sediment-soil dataset (n = 52) and combined water dataset (n = 96) were separately subjected to R-mode factor analysis (R-mFA) to extract the "*factors*" that control the variability in data. Factors are a small number of new latent variables obtained by linearly combining measurements made on the original variables (Davis, 2002; Machiwal et al., 2018). In this study, the "case-to-variable ratio" was kept above five (n/p ≥ 5), as suggested by Bryant and Yarnold (1995). Kaiser criterion (Kaiser, 1960) was used to determine the number of latent factors. The rotation of factors was carried out using the "Varimax raw" method. In this study, factor scores

obtained through *R*-mFA were used to depict the spatial variation of intensity of the geochemical processes, where large negative scores (< -1) indicate areas unaffected by these processes, scores close to zero indicate areas affected to an average degree, and large positive scores ($> +1$) indicate the areas most affected, so called "hotspots" (Lawrence and Upchurch, 1982).

3.3. Spatial data management and data visualization using GIS

In this study, ArcGIS ver. 9.3 and the Spatial Analyst extension (ESRI, 2009) were utilized for general mapping and spatial data management purposes. Thematic maps, showing spatial distribution of PTE concentrations, factor scores (from *R*-mFA), and saturation indices (SI) of the selected mineral phases, were prepared using the simple kriging interpolation algorithm available in the Geostatistical Analyst extension (ESRI, 2009) and employing the procedures outlined by Glendell et al. (2014). GIS data layers used in this study were georeferenced using the UTM projection system (Zone 37N and European Datum 1950). The same projection system was also used when recording the geographic coordinates of the sampling sites, using a handheld GPS unit. Data layers representing geology and fault lines were compiled from the geological maps by Sungurlu et al. (1985) and Çolak et al. (2012). Moreover, map layers depicting streams, lakes, reservoirs, irrigation canals, road network, and land use/land cover (LULC) classes (see Fig. 2) were prepared in GIS by visual interpretation and/or supervised classification of the QuickBird satellite imagery acquired in 2012.

4. Results and discussion

4.1. Arsenic and selected PTEs in stream sediment-soil system

As revealed by the DSİ (2012) survey, the soils of the Uluova plain are mostly alkaline in nature and developed on alluvial-colluvial parent materials eroded from the surrounding mountain slopes. A marked increase in the average soil pH values with depth (i.e. 7.81 at 30 cm, $n = 311$; 7.85 at 60 cm, $n = 307$; 7.90 at 90 cm, $n = 266$; and 7.92 at 120 cm, $n = 209$) is apparent in much of the lower two-third of the basin (DSİ, 2012). Very high soil pH values (in excess of 7.9) are mostly restricted to the central-northern half of the basin (see dashed line in Fig. 1), especially along the line extending from Tadım to Yurtbaşı settlements. This is an important knowledge, since in alkaline soils mobility of As increase substantially (Adriano, 2001), compared to other PTEs (see Table 1), which are generally less mobile and/or bioavailable in a high pH setting (Alloway, 2013). According to USDA (1999) classification, most of the soils are clay loam (47.4%) in character, followed by clay (34.2%), sandy loam (15.2%), and sandy clay (3.2%) (DSİ, 2012). Clays are dominantly found in poorly to moderately drained areas, especially along the Haringet Stream and small tributaries, whereas clay loams occur in areas peripheral to these regions.

The statistical summary of PTE concentrations in the stream sediment and soil datasets are presented in Table 1, where they show significant similarities with respect to their descriptive statistics. In addition, the relative abundances of the PTEs (considering median values) were completely identical for these datasets and ranked in the order of Fe > Al > Mn > Ni > Cr > Zn > Co > As (Table 1). The mean and median concentrations of Fe, Al, and Mn were higher than that of the other PTEs by one to four orders of magnitude (Table 1). Their abundances in the area is most likely related to dominance of Fe–Mn oxyhydroxides and aluminosilicate clay minerals sourced from both alteration of Fe/Mg-rich magmatic/volcanic (silicate) rocks and associated mineralized zones (Fig. 1) containing various sulfide and ferromanganese phases (see Altunbey and Sağıroğlu, 1995; Bölücek et al., 2004; Kaya, 2004; Şaşmaz et al., 2014; Akgul, 2016). The mean concentrations of PTEs (except for Al) in the stream sediment and soil datasets (Table 1) exceeded the crustal averages (Rudnick and Gao, 2014) by a factor of 1.1 to 1.4 for As, Zn, Cr, Mn, and Fe, whereas they ranged from 2.5 to 4.0 for Ni and Co. Nevertheless, the median As and Al concentrations in the stream sediment and soil datasets were lower than that of the European continent agricultural soils median (ECSM) values given by Caritat et al. (2012) (Table 1). The As concentrations (in mg kg^{-1}) in the area range between 0.3 and 13.0 for stream sediment, 0.5–11.7 for "upper" soil, and 0.9–13.0 for "lower" soil samples, which are much lower than the critical As value (30 mg kg^{-1}) recommended for agricultural soils (Kabata-Pendias and Pendias, 2001) (Table 1). The measured As contents of the stream sediment and soil samples from the Uluova basin (Table 1) are in close agreement with the As concentrations observed in magmatic and carbonate rock terrains (see National Research Council, 1977). However, in the stream sediment and soil datasets, PTEs including Ni, Cr, and Co show significant enrichments (Table 1) due to widespread occurrence of mafic and ultramafic lithologies and associated mineralizations (see Fig. 1). Especially, the preferential adsorption by silt- and clay-size fractions and Fe–Mn oxyhydroxides found in the sediment/soil media is known to play an important role in the enrichment of these PTEs (Kabata-Pendias and Pendias, 2001; Abderahman and Abu-Rukah, 2006; Güler et al., 2010). For instance, a fractionation study conducted (Akkus et al., 2013) on soil samples ($n = 12$) collected around the Elazığ airport (see Fig. 2 for location) found that Ni and Cr are prevalently held in silicate-bound (residual) fraction, but they are also significantly

Table 1
Statistical summary of arsenic (As) and selected potentially toxic element (PTE) concentrations (in mg kg^{-1}) in stream sediment (0–15 cm), upper soil layer (0–15 cm), and lower soil layer (15–30 cm) samples from the Uluova basin and their comparison to different reference values from the literature.

	Stream sediment			Soil						Reference values		
Depth	0–15 cm ($n = 28$)			Upper layer: 0–15 cm ($n = 24$)			Lower layer: 15–30 cm ($n = 24$)					
PTE	Range	A.M. ± S.D.	Median	Range	A.M. ± S.D.	Median	Range	A.M. ± S.D.	Median	UCCA[a]	ECSM[b]	MAC[c]
As	0.3–12.4	5.8 ± 3.8	5.8	0.5–11.7	5.5 ± 3.2	4.5	0.9–13.0	6.1 ± 3.4	5.6	4.8	7.0	30
Co	18.0–160.4	69.5 ± 52.5	41.5	10.4–104.7	48.3 ± 26.2	43.5	12.5–115.7	53.2 ± 28.6	44.1	17.3	7.8	50
Zn	32.1–465.0	95.4 ± 106.5	70.4	55.6–104.7	74.5 ± 12.7	75.2	56.1–90.6	75.1 ± 11.6	77.0	67	62	100–300
Cr	23.3–363.1	100.3 ± 64.0	85.2	63.7–262.1	114.6 ± 44.6	101.5	63.4–272.9	116.6 ± 47.6	103.9	92	64	50–80
Ni	53.8–517.7	116.7 ± 86.4	94.0	75.3–236.2	135.9 ± 40.8	128.5	70.9–245.4	138.4 ± 41.0	134.9	47	21	30–75
Mn	344.3–3423.0	889.2 ± 585.0	745.6	627.7–1365.0	920.2 ± 209.0	868.0	641.0–1434.0	926.1 ± 224.0	856.1	774	620	–
Al	14400–40500	24386 ± 7231	22050	20700–35200	27146 ± 4091	27400	20800–37400	27175 ± 4562	27750	81503	55570	–
Fe	39380–55630	46824 ± 3066	46780	37640–48640	44561 ± 2960	45175	39930–50120	45305 ± 3048	45810	39176	25180	–

A.M. ± S.D.: Arithmetic mean ± Standard deviation.
[a] UCCA: Upper continental crust average concentrations (Rudnick and Gao, 2014).
[b] ECSM: European continent agricultural soils median concentrations (GEMAS Ap dataset) (Caritat et al., 2012).
[c] MAC: Maximum allowable concentrations of trace elements in Polish agricultural soils (Kabata-Pendias and Pendias, 2001).

adsorbed onto Fe–Mn oxyhydroxides with amounts ranging from 0.15% to 9.89% for Ni and 2.50% to 11.66% for Cr. Considering the entire stream sediment-soil dataset ($n = 76$), the upper bound of the maximum allowable concentrations (MAC) (Table 1) were exceeded in 89.5%, 69.7%, 39.5%, and 2.6% of the samples for Ni, Cr, Co, and Zn, respectively. This indicates a high potential risk of toxicity with respect to these PTEs (Kabata-Pendias and Pendias, 2001); especially if acidic pH conditions (pH < 7) develop within the soil profile.

The ratio of the "upper" to "lower" soil layer concentrations of individual PTEs (using median values in Table 1) are 0.80 for As, 0.95 for Ni, and range from 0.98 to 0.99 for the rest of the PTEs (i.e. Cr, Co, Al, Zn, and Fe). In the study area, only Mn shows a slight enrichment (with a ratio of 1.01) in the "upper" soil layer. A relatively low ratio of "upper" to "lower" soil layer As concentrations points to active leaching of As from the alkaline soils of the Uluova plain, occurring under natural recharge and agricultural irrigation conditions. Nevertheless, processes such as plant uptake (Gjoka et al., 2011) and low-temperature volatilization (Smedley and Kinniburgh, 2002) could also be partially responsible for the depletion of As in the "upper" soil layer and its relative enrichment in the "lower" soil profile. Whereas, the rest of the PTEs have ratios close to unity, suggesting that they are immobile under present-day alkaline soil conditions (Alloway, 2013) and there is a limited PTE input to the stream sediment-soil system from anthropogenic sources (Facchinelli et al., 2001).

4.2. Factors controlling arsenic and selected PTEs in stream sediment-soil system

In this study, combined stream sediment-soil dataset ($n = 52$), consisting of surficial layer (0–15 cm) samples (Table 1), was subjected to *R*-mFA after data normalization and standardization steps to reveal the possible origins of PTEs and to better understand their interrelationship. K–S normality test results revealed that only Al and Fe had normal distributions, while rest of the PTEs (see Table 2) displayed non-normal distributions requiring transformation. Hence, they were Box-Cox transformed using the Eq. (1) and λ values given in Table 2. Application of *R*-mFA to this dataset (case-to-variable ratio = 6.5) enabled us to extract three latent factors with eigenvalues greater than unity, which collectively explained 70.29% of the total data variance (Table 2). Results obtained from *R*-mFA were evaluated by comparing the maps depicting spatial distribution of individual PTEs (Fig. 3a–h) and factor scores (Fig. 4a–c) to demonstrate their common features in the spatial domain. Table 2 displays the results obtained from *R*-mFA using the combined stream sediment-soil dataset ($n = 52$).

Table 2
R-mode factor analysis results for the combined stream sediment-soil dataset ($n = 52$).[a] Statistically significant loadings (> 0.55) are in bold and underlined (Rotation method: Varimax raw; Extraction method: Principal components).

Variable	Lambda (λ)[b]	Communality[c]	Factor Loadings[d]		
			Factor 1	Factor 2	Factor 3
Al	None	0.748	**0.841**	−0.117	−0.165
As	0.535572	0.906	0.019	−0.124	**0.943**
Co	−0.152574	0.642	−0.226	**0.768**	−0.023
Cr	0.008178	0.823	0.299	**0.836**	−0.183
Fe	None	0.407	**0.588**	−0.083	−0.232
Mn	−0.235320	0.772	**0.838**	0.253	0.071
Ni	−0.578051	0.608	**0.563**	0.537	0.042
Zn	−0.687742	0.718	**0.743**	0.202	0.355
Eigenvalue[e]			3.033	1.507	1.084
Cumulative eigenvalue			3.033	4.540	5.624
Explained variance (%)			37.91	18.83	13.55
Cumulative % of variance			37.91	56.74	70.29

[a] Combined stream sediment-soil dataset is comprised of 28 stream sediment (0–15 cm) and 24 upper soil layer (0–15 cm) samples.
[b] Lambda (λ) is the Box-Cox transformation parameter (see Eq. (1)) used to normalize the stream sediment-soil chemical variables.
[c] Communality is the proportion of a variable's variance explained by the factor model.
[d] Factor loadings, with values ranging from −1 to +1, are the correlation coefficients between the variables (rows) and factors (columns).
[e] Eigenvalue is the amount of the total data variability explained by each factor.

4.2.1. Factor 1: Clay minerals and Fe–Mn oxyhydroxides

Most of the total variance (37.91%) is contained in Factor 1, which is associated with the PTEs that include Al, Fe, Mn, Zn, and Ni, with moderate to strong positive loadings between 0.563 and 0.841 (Table 2). The close spatial and statistical associations between these PTEs (Fig. 3a–e and Table 2) suggest that they share a common source. The association of these PTEs with Factor 1 (Fig. 4a and Table 2) can be explained by their affinity to and occurrence in aluminosilicate clay minerals and Fe–Mn oxyhydroxides (Lindsay, 1979; Bradl, 2004) under favorable soil physico-chemical conditions. Elevated concentrations of Al, Fe, Mn, Zn, and Ni (Fig. 3a–e) and positive Factor 1 scores (between 0.5 and 1.7) (Fig. 4a) are mostly restricted to the SE sector of the Uluova basin, where Elazığ magmatics and Maden complex show extensive distributions (Fig. 1). For instance, Elazığ magmatics is known to host vein-type (Cu-Pb-Zn, Cu, and Fe), skarn-type (Fe and Fe-Ti), and massive sulfide-type (Cu) mineralizations within the breccia zones along the faults and intrusive contacts (Bölücek et al., 2004; Akgul, 2016). In addition, hydrothermal ferromanganese (Fe-Mn) mineralizations occur in different levels of the mudstone member of the volcano-sedimentary Maden complex (Altunbey and Sağıroğlu, 1995; Kaya, 2004; Şaşmaz et al., 2014). Although mineralized zones identified in the Uluova basin (Fig. 1) are small-scale and deemed uneconomical, they are a significant source of several PTEs in the stream sediment-soil system owing to *in situ* natural weathering and pedogenic processes. The presence of well-defined "hotspots" around these mineralizations (Fig. 3a–e) indicate that Factor 1 (Fig. 4a) is mainly controlled by geogenic (natural) sources in the study area.

4.2.2. Factor 2: Weathering of parent materials

Factor 2 explains 18.83% of the total variance and had strong positive loadings on Co and Cr (i.e. 0.768 and 0.836). In Factor 2, Ni also displays a moderate loading value (0.537) that is comparable to the one in Factor 1 (0.563) (Table 2), suggesting that distribution of this trace element may be influenced by multiple sources. For instance, elevated concentrations of Co and Cr in the stream sediment/soil media (Fig. 3f–g) and Factor 2 scores (Fig. 4b) display distinct hotspots, especially in areas covered by Elazığ magmatics and volcano-sedimentary Karabakır formation, both composed of variably altered mafic/ultramafic lithologies (Fig. 1). This suggest that Factor 2 is also controlled by natural processes, such as weathering and alteration of mafic/ultramafic lithologies rich in Co, Cr, and Ni (Güler et al., 2010; Caritat et al., 2012; Alloway, 2013). Sediments/soils derived from these rock types cover much of the Uluova basin (Fig. 1). In the basin, magmatic/volcanic rocks display extremely diverse petrographic compositions (see Perinçek, 1979; Sungurlu et al., 1985; Akgül, 1987, 1993; Yılmaz et al., 1993) and patchy distributions, matching elemental distribution patterns shown in Fig. 3f–g.

4.2.3. Factor 3: Sulfide oxidation in mineralized zones

Factor 3 is a single-element factor, with a strong positive loading (0.943) on As, accounting for 13.55% of the total data variance (Table 2). The lack of any association between As and the other PTEs under Factor 1 and Factor 2 (see Table 2) can be explained by their dissimilar sources and/or behavior within the stream sediment and soil profiles. Elevated As concentrations (Fig. 3h) and Factor 3 scores (Fig. 4c) occur at the northern side of the Uluova basin, along a fault segment running parallel to the Elazığ magmatics (Fig. 1). As it was mentioned earlier, the northern part of the basin (i.e. left side of the

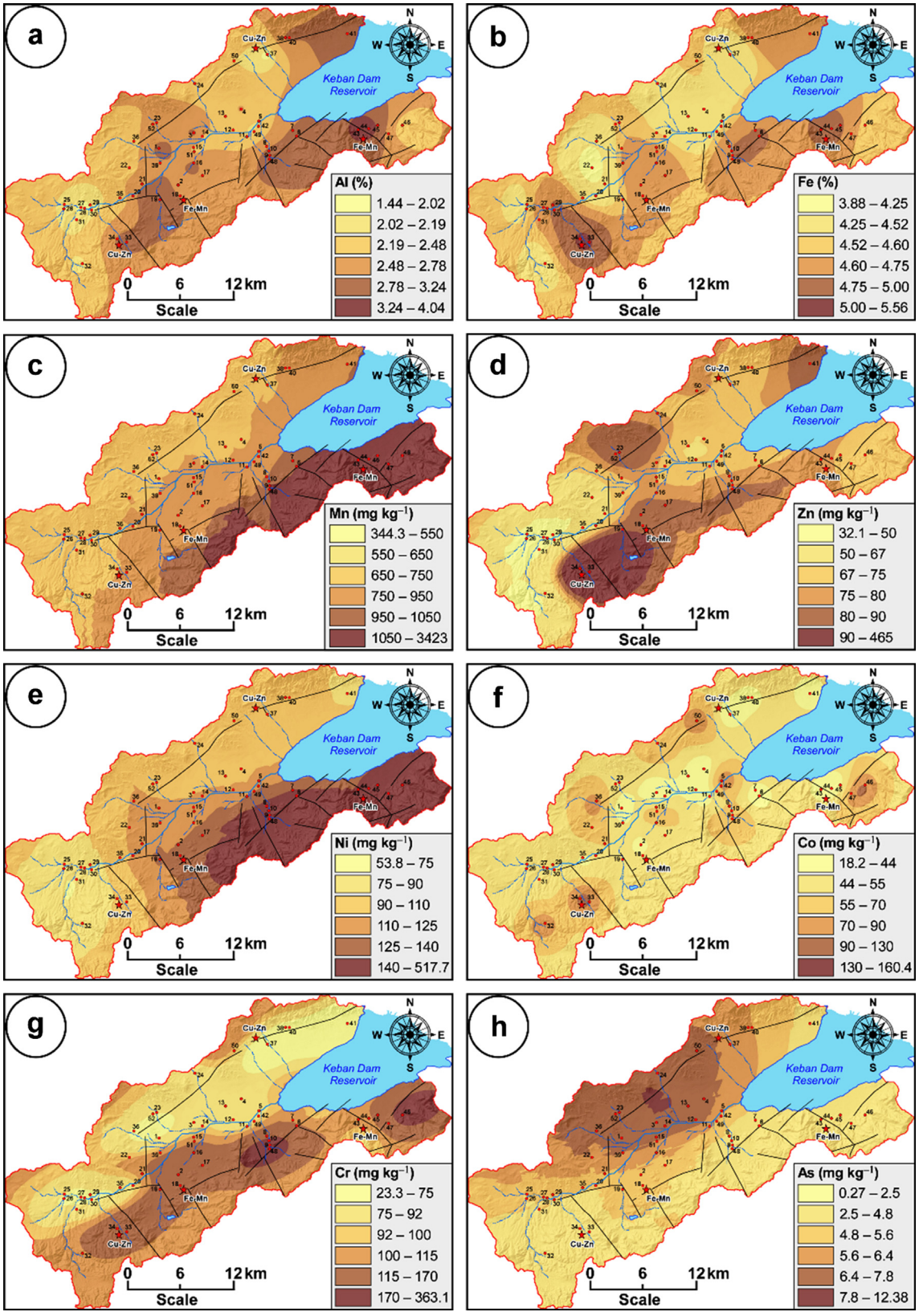

Fig. 3. Estimated spatial distribution of: (a) aluminum (Al, %), (b) iron (Fe, %), (c) manganese (Mn, mg kg^{-1}), (d) zinc (Zn, mg kg^{-1}), (e) nickel (Ni, mg kg^{-1}), (f) cobalt (Co, mg kg^{-1}), (g) chromium (Cr, mg kg^{-1}), and (h) arsenic (As, mg kg^{-1}) concentrations in the combined stream sediment-upper soil layer samples (n = 52; depth 0–15 cm) collected from the Uluova basin. Stream sediment/soil sampling sites and mineralized areas are indicated by red dots and stars, respectively. (For interpretation of the references to colour in this figure legend, the reader is referred to the web version of this article.)

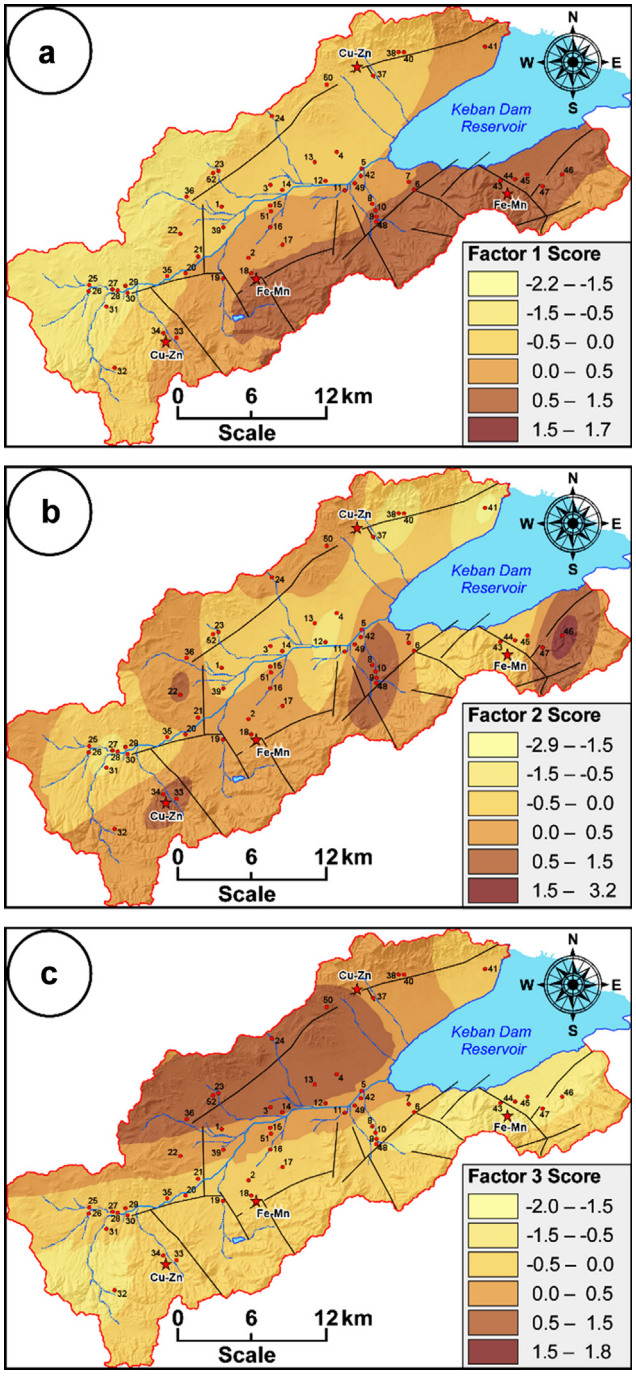

Fig. 4. Maps showing the spatial distribution of the factor scores obtained by *R*-mode factor analysis of the combined stream sediment-soil samples (n = 52; depth 0–15 cm) collected from the Uluova basin: (a) Factor 1: Al, Fe, Mn, Ni, and Zn; (b) Factor 2: Co and Cr; and (c) Factor 3: As. Positive factor scores indicate the areas most affected by the chemical process described by each factor. Stream sediment/soil sampling sites and mineralized areas are indicated by red dots and stars, respectively. Black lines represent faults. (For interpretation of the references to colour in this figure legend, the reader is referred to the web version of this article.)

Haringet Stream) characteristically displays high soil pH values (see Fig. 1) and higher clay contents compared to southern part of the basin (DSİ, 2012), which is possibly an indication of enhanced alteration of rock-forming mafic minerals by fluids circulating within deep penetrating faults or fractures. In the northern part of the basin, vein-type Cu (sulfide) mineralizations with As concentrations reaching up to 1800 mg kg^{-1} have been reported to occur in the fracture systems developed within the Elazığ magmatics (Sagiroglu and Sasmaz, 2004). The primary sulfide phases occurring in these mineralized zones include pyrite, chalcopyrite, arsenopyrite, bornite, galena, and sphalerite, with secondary phases such as limonite, covellite, chalcocite, and cuprite (Bölücek et al., 2004; Akgul, 2016). Oxidation of As-bearing sulfide minerals (e.g. pyrite and arsenopyrite) are probably the main mechanism releasing As (Ravenscroft et al., 2009) to the soil and eventually to the groundwater system in the north-central part of the Uluova basin (discussed in more detail in Section 4.4.1).

Arsenic is also known to occur in the southern part of the basin, within different levels of the Maden complex (Fig. 1), especially in Fe-Mn deposits found within the mudstone member, where reported As concentrations (in mg kg^{-1}) range from 18.6 to 714.3 (mean 205) (Şaşmaz et al., 2014). The primary minerals found in the Fe-Mn mineralized areas are braunite, bixbyite, jacobsite, pyrolusite, manganite, and psilomelane, with variable amounts of limonite, hematite, chromite, barite, and pyrite (Altunbey and Sağıroğlu, 1995; Şaşmaz et al., 2014). However, in this study, no surface expression of elevated As contents has been detected in the stream sediment/soil samples from the southern part of the basin (see Fig. 3h).

4.3. Physico-chemical characteristics of groundwater-surface water system

The descriptive statistics of the groundwater (n = 61), spring water (n = 25), and stream water (n = 10) physico-chemical data, as well as the drinking water quality criteria are presented in Table 3.

4.3.1. Field parameters (temperature, Eh, pH, EC, and DO)

Temperature of the groundwater samples display the widest variation (10.5 °C to 20.2 °C), compared to stream (16.5 °C to 25.9 °C) and spring water samples (16.0 °C to 19.3 °C) (Table 3). The Eh values range from − 55 to 66 mV for groundwater, −61 to 90 mV for spring water, and −70 to 22 mV for stream water samples (Table 3). The pH values of 91 out of 96 water samples are neutral to alkaline in character (between 6.74 and 8.36) and within the permissible limits for drinking water, whereas five samples (nos. 14, 74, 82, 86, and 91; see Fig. 2) have low pH values (between 4.95 and 6.45) and therefore not fit for human consumption (Table 3). The lowest pH value (pH = 4.95) was measured in a stream water sample (no. 91) that is nearby a mineralized zone (Cu-Zn) within the Elazığ magmatics at the SW part of the study area (Figs. 1 and 2). This acidic stream water sample was probably affected by effluents resulting from oxidation of sulfide minerals, as indicated by high concentrations of SO_4^{2-} (200 mg L^{-1}) and PTEs including Al (4438 µg L^{-1}), Cu (727.2 µg L^{-1}), Mn (711 µg L^{-1}), and Ni (32.83 µg L^{-1}). However, low levels of As (0.04 µg L^{-1}) and Fe (67.67 µg L^{-1}) in this water sample suggest that the source probably sulfide minerals other than pyrite and/or arsenopyrite.

In Table 3, wide ranges in electrical conductivity (EC) values is clearly noticeable for different water types, along with rather high standard deviations. Nevertheless, drinking water standard set for EC (EEC, 1998) was only exceeded for three water samples (nos. 14, 74, and 82; see Fig. 2), with values ranging between 2728 and 4770 µS cm^{-1}. The mean value of EC for groundwater samples was higher than that of the spring and stream water samples (Table 3). As indicated by the mean and median dissolved O_2 (DO) concentrations in Table 3, partial oxidizing conditions prevail in the groundwater-surface water system, where 86 out of 96 water samples have DO contents > 5 mg L^{-1}. Lowest DO values (between 1.78 and 4.95 mg L^{-1}) were recorded in the wells (nos. 21–24, 26, 29, 52, and 60) and springs (nos. 79 and 80) located in the lower 2/3 of the alluvial plain (Fig. 2), indicating the presence of local suboxic conditions.

4.3.2. Major ion chemistry

As indicated by the ranges of concentrations and median values given in Table 3, Ca^{2+} and Na^{+} are the dominant cations in water

Table 3
Statistical summary of physico-chemical parameters measured in water samples (n = 96) collected from the Uluova basin and their comparison to current regulations and standards (i.e., water intended for human consumption) set by different organizations.

		Groundwater (n = 61)		Spring water (n = 25)		Stream water (n = 10)		All data (n = 96)	EEC	USEPA	WHO
Parameter	Unit	Range	A.M. ± S.D.	Range	A.M. ± S.D.	Range	A.M. ± S.D.	Median	(1998)	(2009)	(2011)
Temp.	°C	10.5–20.2	16.3 ± 1.8	16.0–19.3	17.6 ± 0.9	16.5–25.9	20.2 ± 3.3	16.75	–	–	–
Eh	mV	−55–66	7.8 ± 21.0	−61–90	7.4 ± 34.0	−70–22	−20.3 ± 32.5	2.00	–	–	–
pH	–	6.3–8.2	7.3 ± 0.3	5.9–8.4	7.3 ± 0.5	5.0–8.3	7.6 ± 1.0	7.38	6.5–9.5	6.5–8.5	–
EC	µS cm^{-1}	159–4080	761.0 ± 607.1	186–4770	670.5 ± 978.9	308–1276	506.6 ± 292.9	533.50	2500	–	–
DO	mg L^{-1}	2.5–8.4	6.2 ± 1.2	1.8–7.8	6.8 ± 1.4	5.4–8.0	6.9 ± 0.7	6.63	5	–	–
Ca^{2+}	mg L^{-1}	10.3–1085.0	72.3 ± 141.9	8.2–419.1	61.8 ± 81.4	26.6–86.1	42.9 ± 18.1	42.90	–	–	–
Mg^{2+}	mg L^{-1}	2.9–395.5	32.2 ± 60.0	4.9–149.9	22.3 ± 31.9	10.6–37.1	19.0 ± 10.0	16.02	–	–	–
Na^{+}	mg L^{-1}	2.9–519.7	41.5 ± 75.8	4.2–578.0	40.9 ± 115.6	6.67–43.3	17.1 ± 12.5	17.22	200	–	–
K^{+}	mg L^{-1}	0.06–42.1	1.9 ± 6.3	0.02–10.2	1.3 ± 2.5	0.13–1.8	0.7 ± 0.6	0.56	–	–	–
Si	mg L^{-1}	0.9–97.8	11.5 ± 12.4	3.1–72.6	11.3 ± 13.0	7.6–11.4	9.4 ± 1.2	8.91	–	–	–
HCO_3^{-}	mg L^{-1}	14.5–4756.8	283.7 ± 651.2	50.7–1836.5	264.3 ± 422.8	49.1–335.7	157.8 ± 84.2	141.91	–	–	–
Cl^{-}	mg L^{-1}	2.8–329.0	44.1 ± 56.7	2.1–313.4	19.6 ± 62.1	1.42–23.4	6.4 ± 6.8	14.18	250	250	–
SO_4^{2-}	mg L^{-1}	2.5–161.0	30.6 ± 26.8	3.0–360.0	28.0 ± 69.6	2.5–200.0	39.6 ± 58.6	18.50	250	250	–
NO_3^{-}	mg L^{-1}	0.8–58.3	12.5 ± 9.3	0.8–37.8	9.8 ± 8.2	0.8–15.9	4.8 ± 4.7	9.25	50	44	50
Al	µg L^{-1}	0.46–2068.0	128.4 ± 318.4	0.46–273.1	34.8 ± 61.8	0.46–4438.0	487.1 ± 1388.6	18.62	200	200	–
As	µg L^{-1}	0.02–367.2	13.6 ± 47.6	0.13–4842.0	203.9 ± 967.0	0.04–31.1	4.9 ± 9.5	1.29	10	10	10
B	µg L^{-1}	5.37–19230	757.1 ± 2602.4	9.61–25260	1377.7 ± 5045.6	17.16–702.8	186.3 ± 229.0	144.15	1000	–	2400
Ba	µg L^{-1}	0.80–2195.0	81.6 ± 288.7	0.62–212.7	33.8 ± 53.3	4.42–59.6	18.9 ± 17.7	22.42	–	2000	700
Br	µg L^{-1}	9.24–13740	527.5 ± 1947.7	14.44–2300	216.7 ± 517.9	16.92–530.5	99.8 ± 167.4	74.06	–	–	–
Cd	µg L^{-1}	0.43–8.6	0.8 ± 1.4	0.43–8.6	0.9 ± 1.8	0.43–4.0	0.8 ± 1.1	0.43	5	5	3
Co	µg L^{-1}	0.15–14.5	0.9 ± 2.0	0.13–3.3	0.4 ± 0.7	0.18–36.6	4.0 ± 11.4	0.23	–	–	–
Cr	µg L^{-1}	0.01–14.2	2.7 ± 2.9	0.01–8.3	0.7 ± 1.8	0.01–5.9	1.0 ± 1.9	0.83	50	100	50
Cu	µg L^{-1}	0.01–14.8	1.4 ± 3.3	0.01–3.0	0.3 ± 0.7	0.01–727.2	73.0 ± 229.9	0.01	2000	1300	2000
Fe	µg L^{-1}	0.01–3473.0	198.7 ± 583.5	0.01–952.1	79.0 ± 203.1	0.01–374.5	69.7 ± 112.6	11.69	200	300	–
Li	µg L^{-1}	0.28–3909.0	78.0 ± 500.5	0.39–295.1	16.9 ± 59.0	0.34–23.3	3.7 ± 7.1	1.73	–	–	–
Mn	µg L^{-1}	0.07–240.7	16.9 ± 44.5	0.07–193.7	13.2 ± 40.2	0.07–711.0	94.6 ± 224.0	1.34	50	50	–
Mo	µg L^{-1}	0.92–42.6	3.0 ± 6.0	0.91–18.3	2.3 ± 4.0	0.90–2.8	1.3 ± 0.5	1.21	–	–	–
Ni	µg L^{-1}	0.16–33.8	2.4 ± 4.8	0.16–8.3	1.6 ± 2.3	0.52–32.8	4.2 ± 10.1	0.85	20	–	70
Pb	µg L^{-1}	0.36–8.8	1.2 ± 1.7	0.36–8.5	0.9 ± 1.7	0.37–0.8	0.5 ± 0.1	0.44	10	15	10
Sb	µg L^{-1}	0.58–156.3	6.2 ± 20.5	0.52–11.0	1.6 ± 2.6	0.71–18.5	3.2 ± 5.6	0.87	5	6	20
Sr	µg L^{-1}	39.81–8218	811.1 ± 1585.4	46.99–2850	470.1 ± 634.1	115.30–537.5	251.8 ± 152.7	323.50	–	–	–
Ti	µg L^{-1}	28.17–2787	187.4 ± 364.9	21.35–1073	159.7 ± 209.7	70.49–221.3	112.0 ± 45.3	110.50	–	–	–
V	µg L^{-1}	0.56–78.4	9.7 ± 11.2	0.26–51.2	8.2 ± 10.2	0.30–10.3	4.9 ± 3.0	6.77	–	–	–
Zn	µg L^{-1}	1.19–674.3	32.3 ± 93.4	1.19–62.9	8.8 ± 14.7	1.27–1099.0	115.0 ± 345.8	3.50	–	5000	–

A.M. ± S.D.: Arithmetic mean ± Standard deviation; Eh: Redox potential; EC: Electrical conductivity; DO: Dissolved oxygen.

samples, followed by Mg^{2+} and K^{+}. Relatively high levels (in mg L^{-1}) of Ca^{2+} (> 100), Na^{+} (> 50), Mg^{2+} (> 50), and K^{+} (> 5) occur in both groundwater and spring water samples and are restricted to the north-central part of the Uluova basin (Fig. 5a). The permissible limit of Na^{+} (200 mg L^{-1}) set by EEC (1998) was exceeded for two groundwater (nos. 14 and 50) and one spring water (no. 74) sample (Fig. 5a), with concentrations between 287 and 578 mg L^{-1}. By far, HCO_3^{-} is the most dominant anion in all water types, where groundwater samples have the highest levels reaching up to 4756.8 mg L^{-1}, followed by spring and stream waters (Table 3). High concentrations (in mg L^{-1}) of HCO_3^{-} (> 250) and SO_4^{2-} (> 50) are restricted to the north-central part of the Uluova basin (Fig. 5b). However, no such trend exists for Cl^{-}; its concentrations vary significantly (Fig. 5b), especially within the area irrigated by the open canal network shown in Fig. 2, where measured Cl^{-} contents reach up to 329 mg L^{-1} (n = 51, mean 50.8 mg L^{-1}). There is a moderate but pervasive nitrate (NO_3^{-}) contamination sourced from anthropogenic activities (e.g. overuse of fertilizers, animal feedlot operations and wastewater discharges) in the UBAS, where only one groundwater sample (no. 17; 58.3 mg L^{-1}) exceeded the drinking water limits (Table 3).

In the UBAS, diverse character of the waters is reflected by the presence of different hydrochemical facies in the Piper diagram (Piper, 1944) (Fig. 6). Thirty-six percent of the groundwater samples are of Ca-Mg-HCO_3 type, along with mixed water types that result from increased abundances of ions such as Na^{+}, Cl^{-}, and/or SO_4^{2-}. Spring water samples are dominated by Ca-Mg-HCO_3 type waters (68%), followed by other hydrochemical facies including Ca-HCO_3, Na-HCO_3, Ca-HCO_3-Cl, Ca-Mg-HCO_3-Cl, Ca-Na-HCO_3, and Ca-Na-HCO_3-SO_4 (Fig. 6). Fifty percent of the stream water samples are also classified as Ca-Mg-HCO_3 type by the Piper diagram (Fig. 6). The rest of the stream water samples are represented by water types of Ca-Mg-HCO_3-SO_4, Ca-Mg-Na-HCO_3, and Mg-Ca-SO_4, resulting from increased dominance of Na^{+} or SO_4^{2-}. The dominance of Ca-Mg-HCO_3 type alkaline waters in the UBAS (n = 44, mean pH 7.41) can be attributed to water-rock interaction processes involving carbonate rocks and mafic/ultramafic lithologies (Güler et al., 2017), which are abundant in the recharge areas (Fig. 1). However, existence of extremely diverse mixed water types, especially in the central portion of the basin-fill aquifer system, cannot be solely explained by the natural factors, as these do not show drastic changes within the Uluova plain. Anthropogenic activities involving: (i) over-exploitation of the aquifer; (ii) extensive hydrologic modifications (e.g. construction of Keban Dam and Eyüpbağları Pumping-Irrigation Project); (iii) discharge of municipal wastewaters; (iv) overuse of fertilizers and animal feedlot operations; and (v) intermittent use of Hazar Lake's saline (EC = 2107 µS cm^{-1}) and alkaline (pH = 9.44) water (Na-Cl-HCO_3 type) in the past for irrigation purposes, probably have not only distorted the natural recharge-discharge equilibrium of the UBAS, but also shifted geochemical equilibrium in the aquifer system (discussed in more detail later).

4.3.3. Arsenic and selected PTEs in groundwater-surface water system

According to their average abundances in the combined water dataset (n = 96) (Table 3), PTEs can be divided into very high (> 100 µg L^{-1}; Sr, B, and Ti), high (10–100 µg L^{-1}; Br, Ba, Al, and Fe), medium (1–10 µg L^{-1}; V, Zn, Li, Mn, As, and Mo), and low (< 1 µg L^{-1}; Sb, Ni, Cr, Pb, Cd, Co, and Cu) concentration ranges. Very high levels of

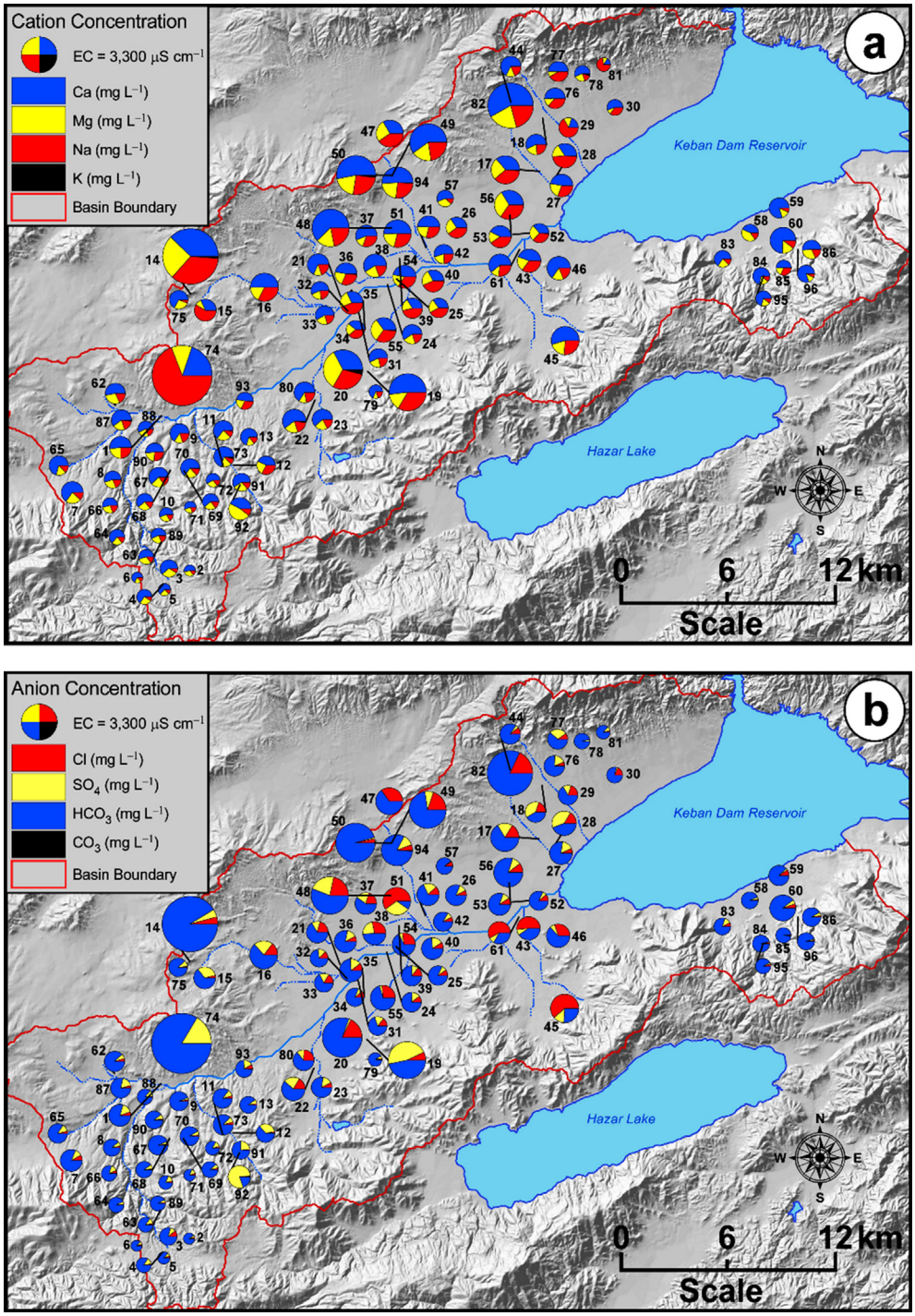

Fig. 5. Pie diagrams representing concentrations of: (a) major cations (Ca^{2+}, Mg^{2+}, Na^{+}, and K^{+}) and (b) major anions (Cl^{-}, SO_4^{2-}, HCO_3^{-}, and CO_3^{2-}) in groundwater (n = 61, nos. 1–61), spring water (n = 25, nos. 62–86), and stream water (n = 10, nos. 87–96) samples collected from the Uluova basin. Radial axis is proportional to the electrical conductivity (EC, µSiemens cm^{-1}) of the water sample. For the combined water dataset (n = 96), total dissolved solids (TDS, mg L^{-1}) is related to the EC (r = 0.9075, p = 0.0000) by the following linear equation: TDS = −66.7674 + 0.69947 × EC.

Sr, B and Ti in water samples can be attributed to water-rock interaction processes, since association of Sr with carbonate rocks (Güler et al., 2017), B with volcanic/volcano-sedimentary rocks (García-Veigas et al., 2011), and Ti with silicate rocks (Hem, 1985) are well known. The concentrations of Cr, Pb, Cu, and Zn in all water samples were below the drinking water criteria (Table 3), most likely due to their low solubilities in alkaline waters (Smedley and Kinniburgh, 2002). No drinking water standards have been established for the seven PTEs (i.e. Br, Co, Li, Mo, Sr, Ti, and V) analyzed in this study (Table 3), hence a comparison cannot be made. In the Uluova basin, 24.6% of the groundwater, 16.0% of the spring water, and 10.0% of the stream water samples have total As concentrations exceeding the current drinking water limit of 10 µg L^{-1} (EEC, 1998; USEPA, 2009; WHO, 2011). Considering all water samples analyzed (n = 96), 5.2% had As contents > 50 µg L^{-1}. In general, As concentrations rarely exceeded the drinking water limits in Ca-HCO_3 and Ca-Mg-HCO_3 type waters, whereas substantial amounts of As were found in Na^{+} and/or Cl^{-} dominated mixed type waters from the UBAS.

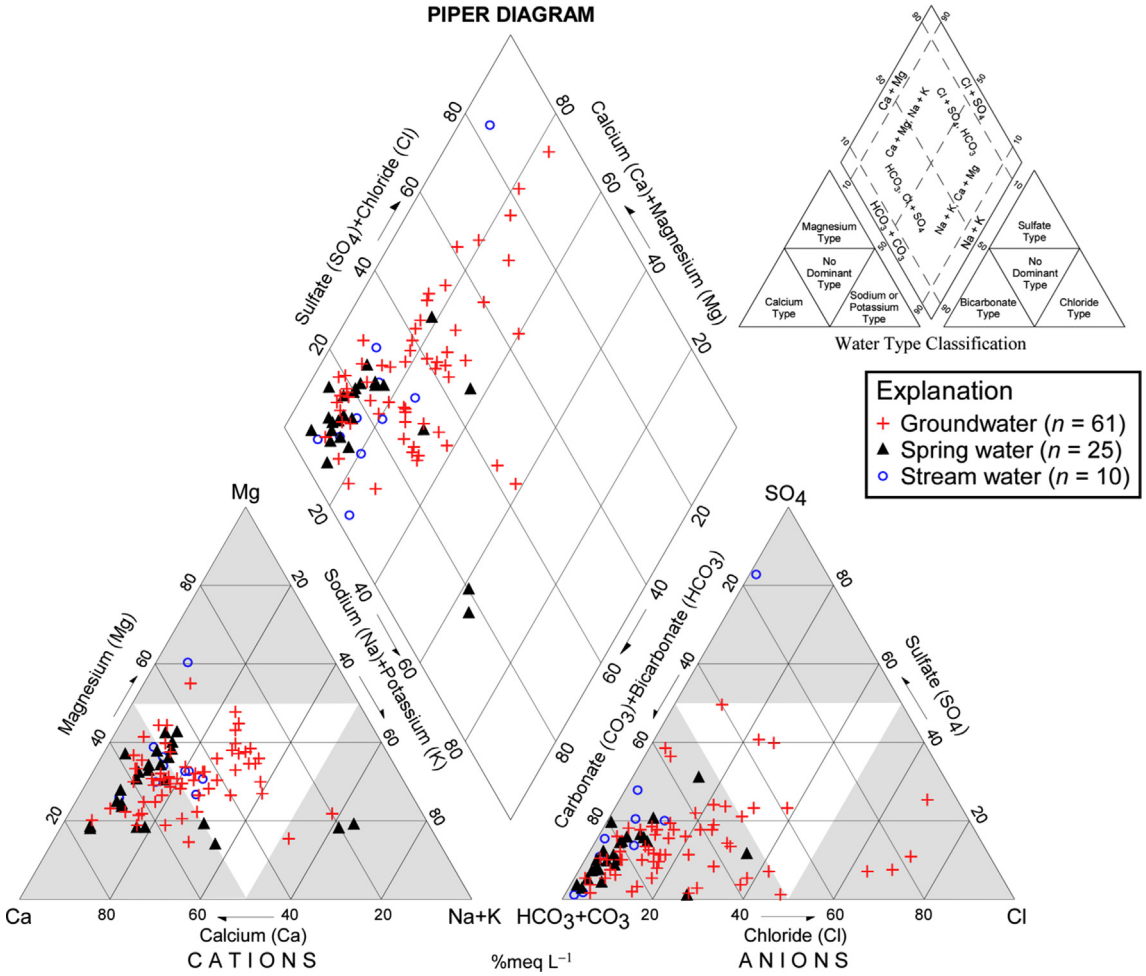

Fig. 6. Piper (1944) diagram illustrating the major ion composition (in %meq L^{-1}) of the water samples (n = 96) collected from the Uluova basin during dry season (October 2013).

In this study, the highest As level measured in sample no. 74 (4842 μg L^{-1}), which belongs to a spring emanating from a contact between Elazığ magmatics and Kırkgeçit sedimentary sequence composed of sandstone, limestone and marl alternations (Figs. 2 and 7a). This spring has a Na-HCO_3 water type and characterized by elevated concentrations of major ions (in mg L^{-1}; Ca^{2+} = 165.2, Mg^{2+} = 92.87, Na^{+} = 578, HCO_3^{-} = 1836.47, and SO_4^{2-} = 360) and trace elements (in μg L^{-1}; B = 25260, Br = 1171, Fe = 952.1, Mn = 193.7, Sr = 1486, and Ti = 449.6) (Fig. 7a–h). Three other springs (nos. 75, 81, and 82; Fig. 2) also displayed high levels of As ranging between 20.18 and 188.8 μg L^{-1} (Fig. 7a and 8). All As-rich springs are located at the northern part of the basin and issue from the above-mentioned geological units.

Out of 61 groundwater samples, 15 have elevated As concentrations ranging from 11.16 to 367.2 μg L^{-1} (Fig. 8). The highest groundwater As content was found in the shallowest well (no. 49; depth 6 m, see inset in Fig. 8) that is located close to northern boundary of the basin (i.e. near the recharge area) (Figs. 2 and 7a). The wells having As levels above drinking water standards are mostly completed within the Quaternary alluvial deposits at the north-central part of the basin (Fig. 7a), with depths ranging from 6 m to 200 m (see inset in Fig. 8). The increase in As contents with decreasing topographic elevation (meters amsl) of water sampling points is evident from Fig. 8 and point out to a inverse relationship. Considering the prevalently oxic nature of groundwaters in both shallow (mean DO = 6.39 mg L^{-1}) and deep wells (mean DO = 5.68 mg L^{-1}) (taking 100 m as an arbitrary boundary), the occurrence of high As levels in deeper aquifer zones (Fig. 8) could be attributed to a recent aquifer cross-contamination, resulting from downward gradient/leakage between aquifers/aquitards, long well screens open to multiple aquifers, and poor well construction (see Santi et al., 2006). Significant tritium (^3H) concentrations (0.2 to 12.1 TU) in shallow and deep wells located in the central part of the UBAS (Çeliker, 2016) also support this hypothesis and confirm the presence of post-1960s water component in samples collected from the wells. Nevertheless, this hypothesis needs further testing through depth specific sampling of both deep aquifer sediments and groundwaters.

The As concentrations in the stream waters range between 0.04 and 31.1 μg L^{-1}, where only one sample (no. 93; Fig. 2) exceeded the current drinking water standard (Table 3). The highest stream water As (31.1 μg L^{-1}), along with the highest water temperature (25.9 °C) (Table 3), occurred in a losing reach of the Haringet Stream, forming a shallow and stagnant pool. The high As level in this water sample (no. 93) has been most likely caused by evapoconcentration of As-laden baseflow feeding the ephemeral channel-pool system. This sampling site (no. 93) is also very close to spring water no. 74 (Fig. 2), exhibiting a record-high natural As content (4842 μg L^{-1}) resulted from sulfide oxidation.

4.4. Factors controlling arsenic and selected PTEs in groundwater-surface water system

R-mFA was applied to combined water dataset (n = 96) to explain the processes governing the distribution of As and selected PTEs in groundwater-surface water system and to better understand their

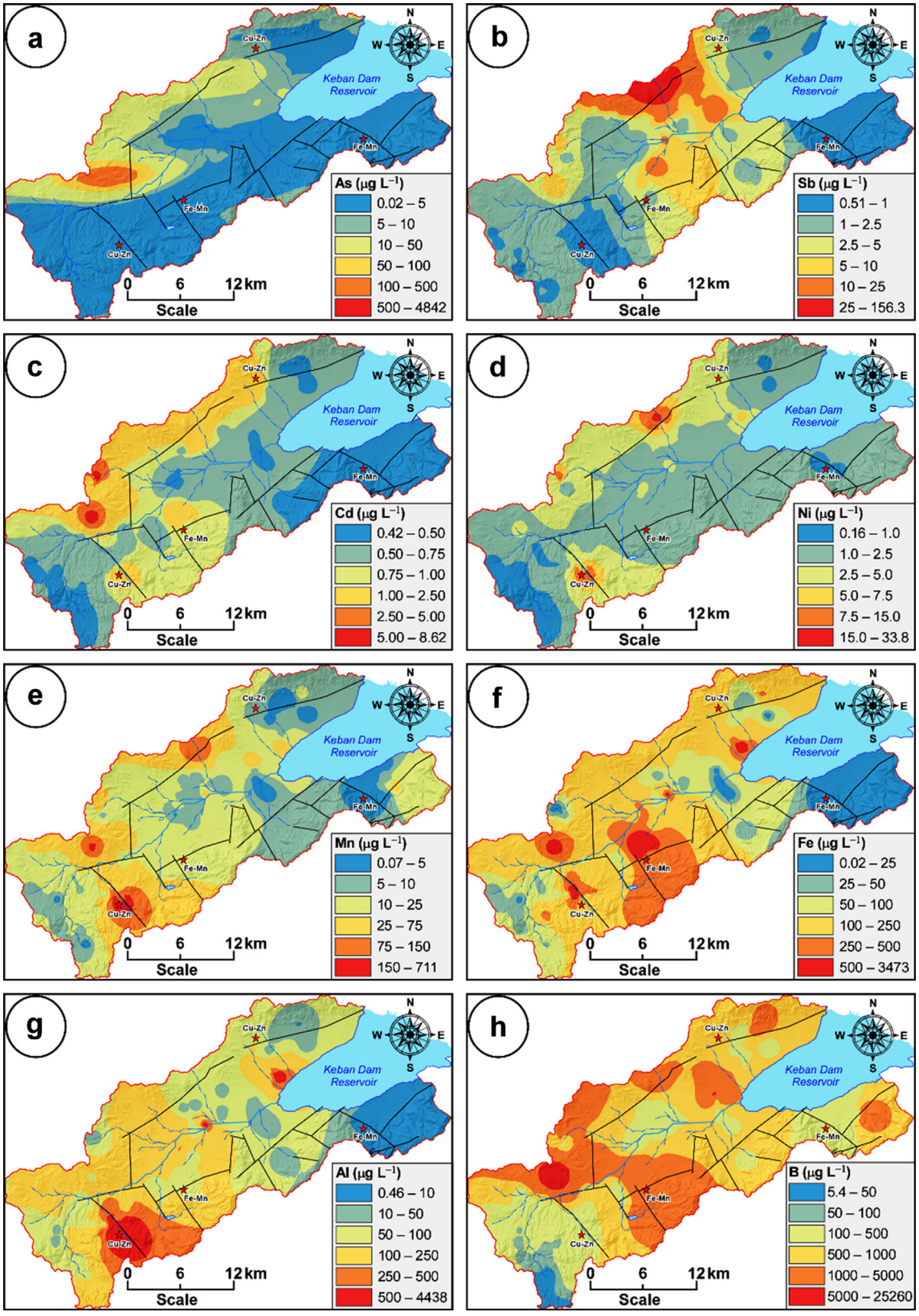

Fig. 7. Estimated spatial distribution of: (a) arsenic (As), (b) antimony (Sb), (c) cadmium (Cd), (d) nickel (Ni), (e) manganese (Mn), (f) iron (Fe), (g) aluminum (Al), and (h) boron (B) concentrations (in μg L^{-1}) in the water samples (n = 96) collected from the Uluova basin. Water sampling sites and their numbers are presented in Fig. 2. Black lines represent faults and stars indicate mineralized areas.

interrelationship. K–S normality test results have shown that Eh is the only variable with a normal distribution, where the rest of the variables showed normal distributions only after various Box-Cox transformations (see Table 4). The variables, including temperature, Ca^{2+}, SO_4^{2-}, Si, Ba, Cd, Co, Cr, Cu, Fe, Pb, Sb, Ti, and V could not be normalized by any means and therefore were excluded from the *R*-mFA.

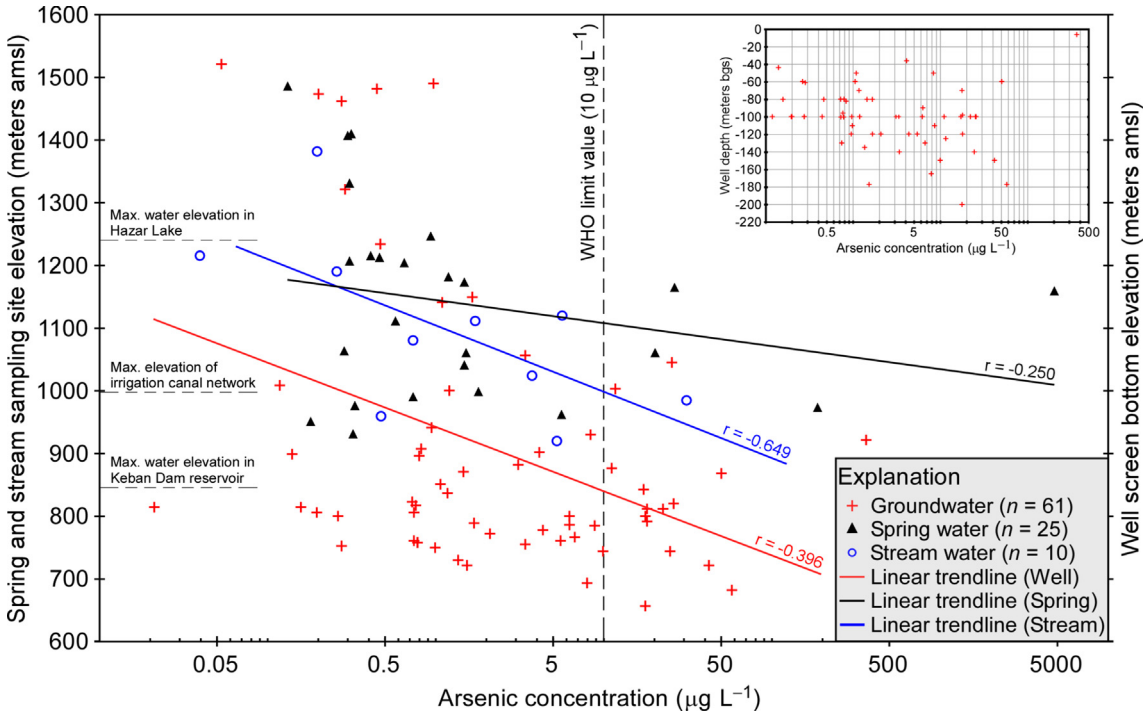

Fig. 8. Scatterplot showing the relationship (i.e., correlation, *r*) between water sampling point elevation above mean sea level (amsl) and arsenic (As) concentrations (in μg L^{-1}) of water samples from the Uluova basin. Elevation values (in meters amsl) denote well screen bottom elevations for groundwater samples, point of emergence for spring water samples, and water sample collection point for stream water samples. Inset shows the relation between well depth (in meters) below ground surface (bgs) and measured As concentrations (in μg L^{-1}) in groundwater samples.

Table 4
R-mode factor analysis results for the combined water dataset (n = 96)[a]. Statistically significant loadings (> 0.59) are in bold and underlined (Rotation method: Varimax raw; Extraction method: Principal components).

			Factor Loadings[d]			
Variable	Lambda (λ)[b]	Communality[c]	Factor 1	Factor 2	Factor 3	Factor 4
pH	4.451411	0.908	−0.101	−0.104	**−0.940**	−0.051
Eh	None	0.848	0.188	0.092	**0.897**	−0.006
DO	2.779764	0.497	−0.293	−0.037	0.102	**−0.632**
Mg	−0.328103	0.795	**0.804**	0.219	0.290	−0.128
Na	−0.252563	0.859	**0.845**	0.140	0.060	0.349
K	−0.122335	0.771	**0.862**	0.148	0.069	0.033
Cl	−0.175526	0.736	**0.601**	−0.045	0.250	0.556
HCO_3	−0.240429	0.722	**0.771**	0.179	0.134	−0.279
NO_3	0.366810	0.463	0.099	0.219	0.128	**0.624**
Al	−0.012881	0.827	−0.020	**0.899**	0.012	0.133
As	−0.110554	0.649	**0.655**	0.176	−0.158	0.405
B	−0.104018	0.812	**0.865**	0.018	−0.002	0.251
Br	−0.275014	0.816	**0.839**	0.019	0.115	0.313
Li	−0.307146	0.641	**0.751**	−0.083	0.197	0.175
Mn	−0.110583	0.791	0.256	**0.834**	0.144	−0.098
Mo	−1.596085	0.595	**0.721**	0.142	0.065	0.224
Ni	−0.252818	0.706	**0.650**	0.457	0.269	−0.039
Sr	−0.158345	0.835	**0.895**	0.067	0.170	0.033
Zn	−0.500000	0.521	−0.173	**−0.599**	−0.304	−0.197
Eigenvalue[e]			8.679	2.241	1.586	1.286
Cumulative eigenvalue			8.679	10.919	12.505	13.791
Explained variance (%)			45.677	11.794	8.346	6.769
Cumulative % of variance			45.677	57.470	65.817	72.586

Eh: Redox potential; EC: Electrical conductivity; DO: Dissolved oxygen.
[a] Combined water dataset is comprised of 61 groundwater, 25 spring water, and 10 stream water samples.
[b] Lambda (λ) is the Box-Cox transformation parameter (see Eq. (1)) used to normalize the water physico-chemical parameters.
[c] Communality is the proportion of a variable's variance explained by the factor model.
[d] Factor loadings, with values ranging from −1 to +1, are the correlation coefficients between the variables (rows) and factors (columns).
[e] Eigenvalue is the amount of the total data variability explained by each factor.

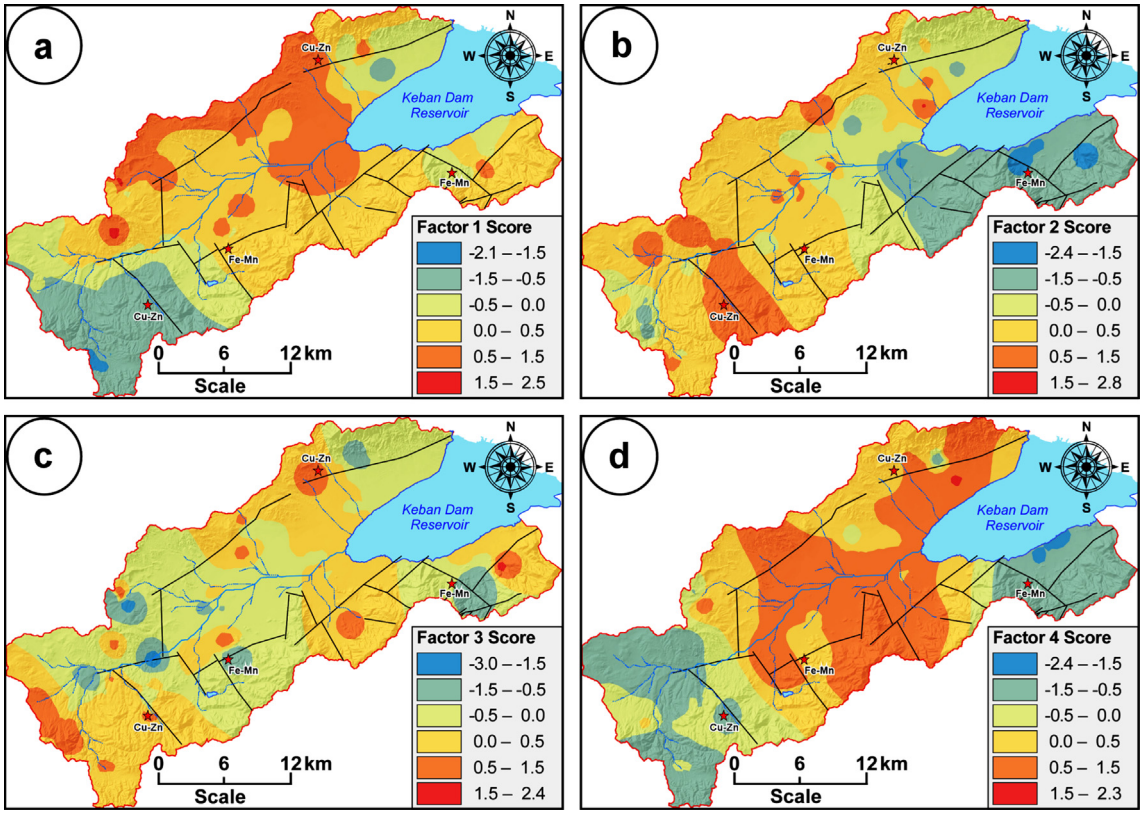

Fig. 9. Maps showing the spatial distribution of the factor scores obtained by *R*-mode factor analysis of the water samples (n = 96; 61 groundwater, 25 spring water and 10 stream water) collected from the Uluova basin: (a) Factor 1: Mg^{2+}, Na^{+}, K^{+}, Cl^{-}, HCO_3^{-}, As, B, Br, Li, Mo, Ni, and Sr; (b) Factor 2: Al, Mn, and Zn; (c) Factor 3: pH and Eh; and (d) Factor 4: DO and NO_3. Positive factor scores indicate the areas most affected by the chemical process described by each factor. Black lines represent faults and stars indicate mineralized areas.

For that reason, nonparametric Spearman rank order correlations were also calculated (not shown) for all variable pairs to aid the interpretation of the results from the *R*-mFA. The results of the *R*-mFA for combined water dataset are presented in Table 4. The final *R*-mFA model included 19 physico-chemical variables (pH, Eh, DO, Mg^{2+}, Na^{+}, K^{+}, Cl^{-}, HCO_3^{-}, NO_3^{-}, Al, As, B, Br, Li, Mn, Mo, Ni, Sr, and Zn) measured in 96 water samples (case-to-variable ratio = 5.05), which were combined into four latent factors explaining 72.59% of the total variance in the dataset (Table 4). Maps depicting spatial distribution of parameter values (e.g. Figs. 5 and 7a–h) and factor scores (Fig. 9a–d) were also used to interpret the results from the *R*-mFA (Table 4).

4.4.1. Factor 1: Groundwater salinization and arsenic mobilization

Factor 1, accounting for 45.68% of the total variance, is strongly associated with the variables Mg^{2+}, Na^{+}, K^{+}, Cl^{-}, HCO_3^{-}, As, B, Br, Li, Mo, Ni, and Sr, which all display positive loading values ranging from 0.601 to 0.895 (Table 4). Factor 1 is comprised of hydrochemical variables that typically originate from natural water-rock interaction processes of magmatic/volcanic and sedimentary series found in the recharge areas and/or in the basin-fill deposits (see Fig. 1). For instance, associations between these variables can be explained by dissolution of carbonate rocks (source of Ca, Mg, and Sr), weathering of silicate rocks (source of Al, Fe, Mg, Mn, Si, Co, Cr, Ni, Ti, and Zn), oxidation of sulfide minerals (source of As, Cu, Mo, Pb, Sb, and V), and dissolution of evaporitic minerals and/or ion exchange in clays (source of Na^{+}, K^{+}, Cl^{-}, B, Br, and Li) (Hem, 1985; Güler et al., 2012). Especially, the latter suite of elements are important, since they indicate the presence of a natural salinization phenomenon (i.e. water-rock interaction) and/or a saline water component in the area.

Elevated aqueous As levels (Fig. 7a) and Factor 1 scores ranging from 0.5 to 2.5 (Fig. 9a) occur in the central-northern half of the Uluova basin, which is characterized by very high soil pH values (Fig. 1), clay contents, and slightly higher soil As concentrations (Fig. 3h). Water samples from the central-northern half of the basin also display remarkably high major ion (Fig. 5a and b) and trace element (Fig. 7a–h) concentrations. To shed light onto hydrogeochemical processes occurring in the UBAS, saturation indices (SI) of the selected mineral phases (calculated by PHREEQCI) were separately interpolated by simple kriging method to reveal their spatial distributions (see Fig. 10a–h). The hydrogeochemical data suggest that, under prevailing alkaline and partial oxidizing conditions (Table 3), two separate but closely related mechanisms are likely responsible for the As mobilization in the UBAS. These mechanisms are: (i) oxidation of As-containing sulfide phases found within the fault/fracture zones associated with the Elazığ magmatics in the upland areas at north and (ii) subsequent cyclic As adsorption-desorption to/from aquifer media (consisting of surface reactive solid phases such as clays and Fe–Mn oxyhydroxides) along the downgradient groundwater flow path, subject to constantly changing (in a spatiotemporal sense) physico-chemical conditions due to natural and/or human-induced perturbations. In the area, the former mechanism plays a pivotal role in the As-enrichment of all water types. For instance, in the mountain watersheds, oxidation of As-bearing sulfide phases (e.g. pyrite and arsenopyrite) plays a critical role in As-enrichment of the fractured rock aquifers, since they are thermodynamically unstable under oxidizing conditions (Peters et al., 1999; Nordstrom, 2000). Pyrite, especially arsenian pyrite, is known to contain significant amounts of As (0.02% to 0.5%) in solid solution (National Research Council, 1977). Oxidation of these As-bearing sulfides leads to formation of Fe oxyhydroxides and release of sulfate [SO_4^{2-}], arsenate [As (V)], and acidity [H^{+}] into the aqueous phase (Smedley and Kinniburgh, 2002) according to Eqs. (2) and (3):

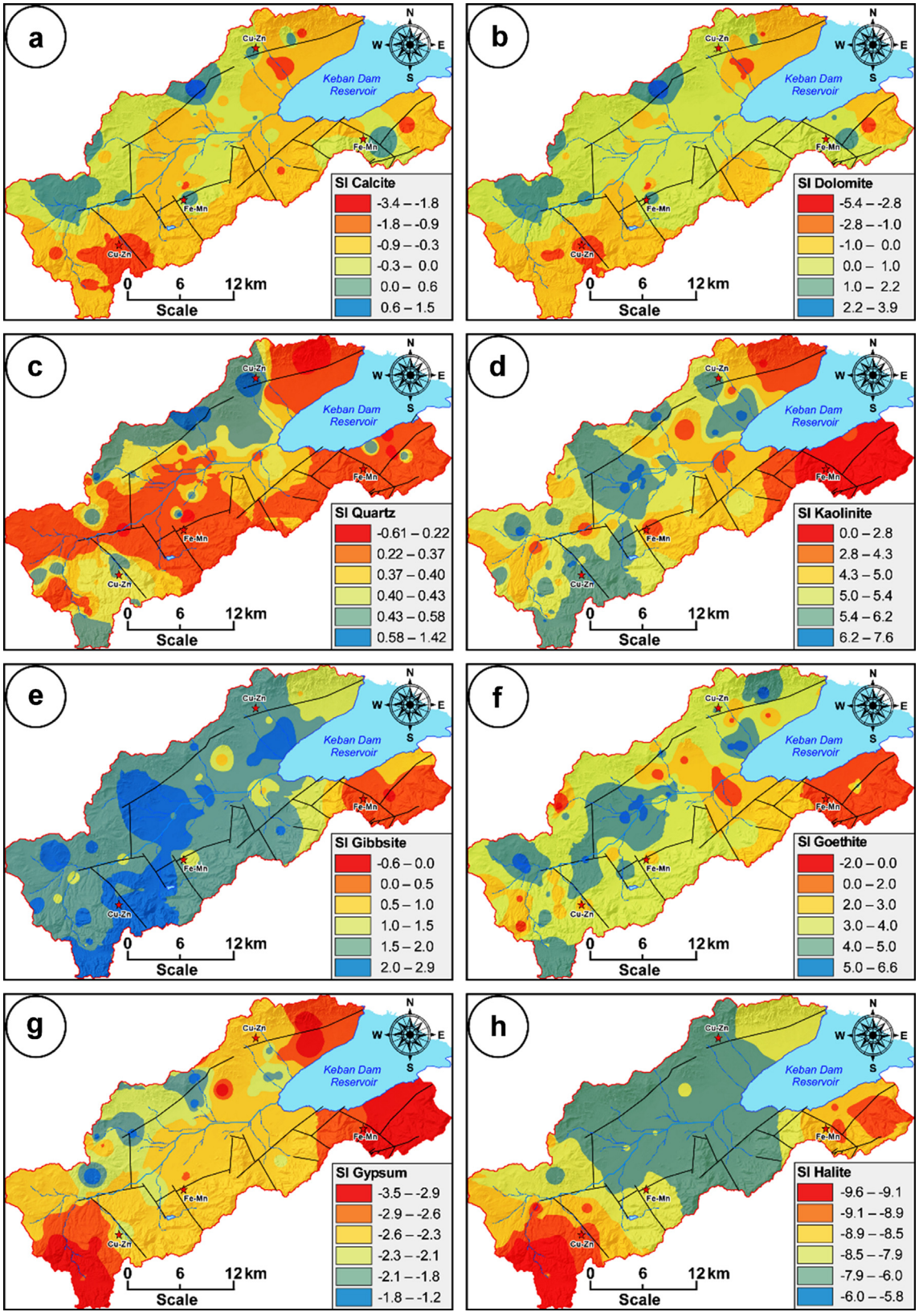

Fig. 10. Maps showing the spatial distribution of PHREEQCI (Parkhurst and Appelo, 2015) calculated saturation indices (SI) for the selected mineral phases: (a) calcite [$CaCO_3$], (b) dolomite [$CaMg(CO_3)_2$], (c) quartz [SiO_2], (d) kaolinite [$Al_2Si_2O_5(OH)_4$], (e) gibbsite [$Al(OH)_3$], (f) goethite [FeOOH], (g) gypsum [$CaSO_4{\cdot}2H_2O$], and (h) halite [NaCl]. Water sampling sites and their numbers are presented in Fig. 2. Black lines represent faults and stars indicate mineralized areas. SI = log [IAP/K_{eq}]; where IAP and K_{eq} represent ion activity product and equilibrium constant, respectively.

$$FeS_2\ (\text{Pyrite}) + \frac{15}{4}O_2 + \frac{7}{2}H_2O \rightarrow Fe(OH)_3 + 2SO_4^{2-} + 4H^+ \quad (2)$$

$$\text{FeAsS (Arsenopyrite)} + \frac{7}{2}O_2 + 4H_2O \rightarrow Fe(OH)_3 + SO_4^{2-} + H_2AsO_4^- + 3H^+ \quad (3)$$

Arsenate released, in turn, will be adsorbed onto clays and Fe–Mn oxyhydroxides (Smedley and Kinniburgh, 2002; Mukherjee et al., 2014) when conditions become suitable. Acidity generated by the reactions given above (Eqs. (2) and (3)) is most likely buffered through water-rock interaction of carbonates (Eqs. (4) and (5)) and ferromagnesian minerals (Eq. (6)) found along the flow path in the aquifer system:

$$CaCO_3(Calcite) + H^+ \leftrightarrow Ca^{2+} + HCO_3^- \quad (4)$$

$$CaMg(CO_3)_2(Dolomite) + 2H^+ \leftrightarrow Ca^{2+} + Mg^{2+} + 2HCO_3^- \quad (5)$$

$$Mg_2SiO_4(Forsterite) + 4H^+ \rightarrow 2Mg^{2+} + H_4SiO_4^0 \quad (6)$$

Calculated SI values for both calcite and dolomite (mean values are −0.40 and 0.14, respectively) are mostly positive and decrease along the groundwater flow path (Fig. 10a and b) in the northern half of the basin, whereas they are mostly undersaturated or in equilibrium at the southern half. Decrease in calcite and dolomite SI values along the flow path can be explained by different mechanisms, including precipitation of the respective mineral phases and/or dilution/mixing with a fresh-water component, both of which are likely to be important in the UBAS. Considering that soils and sediments from the central-northern part of the UBAS have high clay contents (DSİ, 2012), ion exchange reactions (Eq. (7)) may also be partially responsible for the decrease in Ca^{2+} and Mg^{2+} and the increase in Na^+ concentrations along the flow path (Domenico and Schwartz, 1997) as shown below:

$$Ca^{2+}(or\ Mg^{2+}) + 2Na - clay \leftrightarrow 2Na^+ + Ca(or\ Mg) - clay \quad (7)$$

Except for a few cases, all water samples from the area remain supersaturated with respect to quartz, kaolinite, gibbsite, and goethite, with mean SI values of 0.39, 4.89, 1.74, and 3.39, respectively (Fig. 10c–f). Especially, around Cu-Zn mineralized areas found within the Elazığ magmatics (Fig. 1), SI values of quartz, kaolinite (as well as beidellite and smectite type clays) and metal oxyhydroxides (gibbsite and goethite) display similar spatial patterns and high values (Fig. 10c–f), which can be attributed to enhanced water-rock interaction of mafic/ultramafic rocks by acidity generated from sulfide oxidation (see Eqs. (2) and (3)). Under oxidizing and circumneutral pH conditions, the secondary mineral phases (e.g. clays and metal oxyhydroxides) attain positive surface charge, which facilitates the adsorption of anionic As species (e.g. arsenates) (Smedley and Kinniburgh, 2002; Scanlon et al., 2009). However, with increasing pH, the surface charge of clays and metal oxyhydroxides becomes negative, leading desorption of arsenates [As(V)] and their subsequent release into the aqueous phase (Smedley and Kinniburgh, 2002). In the UBAS, all water samples remain highly undersaturated with respect to gypsum and halite (see Fig. 10g and h), suggesting that dissolution of these minerals are favored in the aquifer (see Eqs. (8) and (9)), as follows:

$$NaCl(Halite) \leftrightarrow Na^+ + Cl^- \quad (8)$$

$$CaSO_4 \cdot 2H_2O(Gypsum) \leftrightarrow Ca^{2+} + SO_4^{2-} + 2H_2O \quad (9)$$

The highest gypsum SI values ($-2.3 < SI < -1.2$) occur in the northern half of the basin (Fig. 10g), where water samples with high major ion concentrations are known to occur (see Fig. 5a and b). However, halite saturation display a unique pattern in the central-eastern part of the basin, irrigated by the canal network (see Fig. 2), where SI values ($-8.5 < SI < -5.8$) (Fig. 10h), as well as Na^+ and Cl^- contents (Fig. 5b), are higher compared to other parts of the basin. Natural water-rock interaction processes represented by Eqs. (2)–(9), play an important role in the increase of groundwater salinity (dissolved ions) and alkalinity, especially in closed/semi-closed basins found in arid/semiarid environments (Güler and Thyne, 2004; Güler et al., 2012).

As it was mentioned previously, intermittent use of saline (Na-Cl-HCO_3 type) water (between 1988 and 2006) from Hazar Lake for agricultural irrigation (Çetindağ and Okan, 2004; Çeliker, 2008) may have also contributed to the salinization in the central-eastern (canal-irrigated) part of the Uluova plain (see Fig. 2). The Hazar Lake water sample (EC = 2107 μS cm^{-1} and pH = 9.44) analyzed in this study was found to contain elevated concentrations of Na^+ (405.2 mg L^{-1}), Cl^- (380 mg L^{-1}), K^+ (7.01 mg L^{-1}), B (1768 μg L^{-1}), Br (2615 μg L^{-1}), and As (17.49 μg L^{-1}), clearly indicating its saline character. Use of Hazar Lake's water in the past for irrigation purposes, probably have not only contributed to the salinization of the UBAS, but also added a significant amount of As to already As-enriched central-eastern part of the basin. Furthermore, complex human interventions, including land use changes, overexploitation and re-circulation of groundwater (causing evapoconcentration) by pumping, irrigation return flow, overuse of agrochemicals, animal feedlot operations, construction of large dams (Keban), massive irrigation structures (Eyüpbağları Pumping-Irrigation Project) and hydroelectric facilities (Hazar I and II HEPPs), and wastewater discharges have probably not only disrupted natural surface/subsurface flow and solute transport mechanisms, but also led entrapment of salts from these artificial inputs and natural inflows (e.g. water-rock interaction and meteoric salt deposition), causing enhanced water mineralization and internal salinization of the semi-closed UBAS under prevailing semiarid climate conditions.

The saline, alkaline and oxygen-rich nature of the groundwaters in the UBAS may lead to enhanced As enrichment through competitive desorption driven by increased groundwater ionic strength (e.g. Scanlon et al., 2009). For instance, under alkaline, oxidizing and high ionic strength aquifer conditions, inorganic oxyanions (e.g. SO_4^{2-}; HCO_3^-, CO_3^{2-}, NO_3^-, PO_4^{3-} and of Si, As, B, Mo, Se, Sb, V, and U) compete for sorption sites on clays and Fe–Mn oxyhydroxides, enhancing further As release (e.g. $HAsO_4^{2-}$ and $H_2AsO_4^-$) into groundwater (Goldberg et al., 2008; Scanlon et al., 2009; Raychowdhury et al., 2014). In the UBAS, the oxyanions HCO_3^-, SO_4^{2-} and of Si, B, Mo, Sb and V are of particular concern due to their relative abundance in water samples from the central-northern half of the basin. Statistically significant (at $p = 0.05$ level) Spearman rank order correlations between these co-genetic oxyanions and As (ρ values between 0.39 and 0.69) suggest that competitive desorption may be an important process in the enhanced mobilization of As, as well as other inorganic oxyanions in the UBAS.

4.4.2. Factor 2: Clay minerals and Fe–Mn oxyhydroxides

The second factor (Factor 2), explaining 11.79% of the total data variance, has high positive loadings on Al (0.899) and Mn (0.834), and a moderately negative loading on Zn (−0.599) (Table 4). Elevated concentrations of these PTEs (including Fe) (Fig. 7e–g) and positive Factor 2 scores (Fig. 9b) are mostly restricted to the SW sector and central-northern half of the basin, especially around mineralized zones within Elazığ magmatics and Maden complex (Fig. 1). Similar to *R*-mFA results from the combined stream sediment-soil dataset (Section 4.2), the association of these PTEs with Factor 2 (Table 4) can be explained by their close relation with aluminosilicate clay minerals and Fe–Mn oxyhydroxides, which are found to be supersaturated in the great majority of water samples (Fig. 10d–f). These surface reactive mineral phases probably act both as sink and source for As (Smedley and Kinniburgh, 2002) in the UBAS, controlling its concentration and mobility in groundwater. However, their activities are mainly governed by the redox state and pH level of the groundwater (Peters et al., 1999). Statistically significant (*p* level 0.05) Spearman rank order correlations between Al, Fe, and Mn (ρ values between 0.72 and 0.81) suggest that these PTEs have similar behavior and sources. Water-rock interactions involving parent rocks (i.e. Elazığ magmatics and Maden complex) and associated small-scale mineralizations (i.e. Cu-Zn and Fe-Mn) appear to

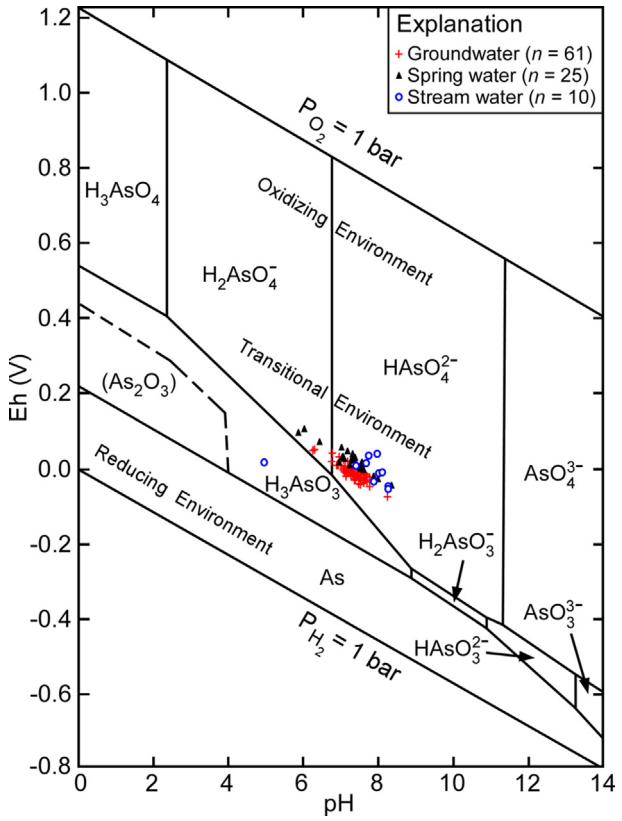

Fig. 11. Distribution of water samples (n = 96) collected from the Uluova basin on the Eh-pH (Pourbaix) diagram for As–O–H system at 25 °C (298.15 K) and 1 bar (10^5 Pa) pressure, where total activity of dissolved As = 10^{-6} M (modified after Brookins, 1988). The upper and lower stability limits of water (H_2O) are given where PO_2 and PH_2 = 1 bar, respectively.

be the primary factor governing the abundance and distribution of these PTEs in the UBAS (Fig. 7e–g).

4.4.3. Factor 3: pH and redox (Eh) conditions

Factor 3, accounting for 8.35% of the total data variance, has a high negative factor loading (−0.940) for pH and a high positive factor loading (0.897) for redox potential (Eh) (Table 4). In the study area, the lowest pH values (4.95–6.45), caused by oxidation of sulfides, typically occur around Cu-Zn mineralized zones found within the Elazığ magmatics, whereas the highest pH values (7.50–8.36) are restricted to the areas of hydrothermal ferromanganese (Fe-Mn) mineralizations associated with the volcano-sedimentary Maden complex (see Fig. 1). However, Eh values display an opposite trend, which is quite similar to Factor 3 score distribution map in Fig. 9c. Distinct hotspots in Fig. 9c, characterized by Factor 3 scores ≤ −0.5 (observed around Fe-Mn mineralizations) and ≥0.5 (observed around Cu-Zn mineralizations), can be linked to the natural weathering processes in mineralized zones, some of which possibly have not been identified to date. pH and Eh are important properties governing the inorganic As speciation in sediment-soil and groundwater-surface water systems (Brookins, 1988; Peters et al., 1999; Smedley and Kinniburgh, 2002). Therefore, pH and Eh values measured *in situ* were plotted on the Pourbaix diagram (Fig. 11) to determine dominant As species found in the UBAS. As indicated by Fig. 11, water samples plot mainly in the stability fields of $HAsO_4^{2-}$ and $H_2AsO_4^-$, both of which arsenate [As(V)] species that commonly occur under alkaline and oxidizing conditions. Except for a few cases, water samples from the UBAS is alkaline in character and under partially oxidizing conditions, as indicated by the relatively high median pH and DO values (Table 3). One stream water sample (no. 91), however, plot in the stability field of arsenite [As(III)] species H_3AsO_3 (Fig. 11). As discussed previously, this stream water sample (no. 91) has the lowest pH value (4.95) and probably affected by the effluents resulting from oxidation of sulfides. PHREEQCI (Parkhurst and Appelo, 2015) speciation calculations have shown that in the water samples (n = 96), As mainly occurs in the form of inorganic As(V) oxyanions $HAsO_4^{2-}$ (94.8%) and $H_2AsO_4^-$ (5.2%), with median molalities of 1.34×10^{-8} and 2.72×10^{-9}, respectively. These results are in agreement with the field measured Eh and pH values (Fig. 11). The speciation calculations also revealed that total As(III) in water samples is extremely low, with a median molality of 6.29×10^{-17}.

4.4.4. Factor 4: Aquifer oxygenation and nitrate contamination

Factor 4 explains 6.77% of the total data variance and is related to DO and NO_3^-, with loadings of −0.632 and 0.624, respectively (Table 4). In the UBAS, association of these electron acceptors with Factor 4 is not surprising, considering the prevailing oxidizing conditions and the presence of nitrate contamination from anthropogenic sources (e.g. overuse of fertilizers, animal feedlot operations and wastewater discharges). Oxygen-rich nature of the UBAS can be attributed to both natural and anthropogenic processes, including meteoric recharge, groundwater drawdown during dry season, heavy groundwater pumping, induced recharge from agricultural irrigation and O_2-rich surface waters (e.g. Haringet Stream, Keban Dam, and Hazar Lake). These hydrological processes or activities most likely led to spatio-temporally varying fluctuations in groundwater levels, enhanced groundwater flow, and aeration/oxygenation of the aquifer media (water and sediments). In agriculture dominated parts of the Uluova basin (see Fig. 2), DO and NO_3^- concentrations display a very similar spatial pattern that resemble to Factor 4 score distribution map shown in Fig. 9d. Especially, the areas enclosed by Factor 4 scores between 0.5 and 2.3 (Fig. 9d) are the parts most affected by the NO_3^- contamination. In general, NO_3^- concentrations gradually decrease away from the agricultural areas and display rather low concentrations ($\leq$12 mg L^{-1}) in areas covered by non-agricultural land use classes (see Fig. 2). The highest NO_3^- concentrations (up to 58.3 mg L^{-1}) are restricted to the north-eastern part of the Uluova plain, especially around Yurtbaşı and Sedeftepe settlements (see Fig. 2), where the use of chemical fertilizers and organic manures in agriculture is a common practice (Çetindağ and Okan, 2004).

5. Conclusions

Studies dealing with arsenic (As) occurrence and distribution in the stream sediment-soil and groundwater-surface water systems of Eastern Turkey are extremely rare, if nonexistent. In this study, we aimed to provide a general view of the hydrologic and geochemical conditions conducive to As release from the aquifer media and its subsequent mobility in the Uluova basin aquifer system (UBAS) (Elazığ province, Eastern Turkey) utilizing an integrated approach. GIS mapping, geostatistics, multivariate statistical analysis and geochemical modeling techniques have been used in an integrated manner to illustrate the basinwide distribution of the selected potentially toxic elements (PTEs), to identify hotspot areas and levels of contamination, to examine associations between data variables, and to deduce factors affecting stream sediment-soil and groundwater-surface water chemistries in the UBAS. As revealed by the geochemical results, As concentrations in the stream sediment-soil system are typically low and in the range 0.3 to 13 mg kg^{-1}. Sediments/soils from the area are highly alkaline in nature and enriched in Ni, Cr, and Co due to abundance of mafic and ultramafic lithologies. Elemental associations revealed by the R-mFA of stream sediment-soil dataset indicated that the secondary mineral phases (clays and Fe–Mn oxyhydroxides), weathering of parent materials, and sulfide oxidation in mineralized zones are the main factors controlling the spatial distribution and concentrations of PTEs in the UBAS. On the other hand, As contamination in groundwater-surface water system of the UBAS is much more extensive than previously

believed and driven by interaction of complex processes related to local geology, geomorphology, tectonic activity, climatic conditions, sediment/soil geochemistry, hydrogeology of the fractured rock and basin-fill aquifers, and human-induced perturbations to the aquifer system causing internal salinization and oxidation. Under prevailing semiarid climate and alkaline soil/water conditions, oxidation of small scale (vein-type) mineralized zones (containing sulfides) associated with the fractured rock aquifers (i.e. Elazığ magmatics) and water-rock interaction processes occurring along the downgradient groundwater flow path play an important role in the enrichment of As and other oxyanion-forming elements (e.g. HCO_3^-, SO_4^{2-} and of Si, B, Mo, Sb and V) in groundwater from the UBAS. Competitive alkaline desorption and ion exchange reactions involving surface reactive phases (clays and Fe–Mn oxyhydroxides) also control As mobility. In the UBAS, elevated As concentrations are confined into north-central part of the basin and mainly occurs as inorganic As(V) species (i.e. $HAsO_4^{2-}$ and $H_2AsO_4^-$), which are known to be 25–60 times less toxic than As(III) species. In the UBAS, the highest total As concentrations measured in Na^+ and/or Cl^- dominated mixed type spring water (up to 4842 $\mu g\,L^{-1}$) and groundwater (up to 367.2 $\mu g\ L^{-1}$) samples, where 20.83% of the sampled waters exceeded the WHO provisional guideline value (i.e. 10 $\mu g\,L^{-1}$).

Anthropogenic activities involving overexploitation of the aquifer, extensive hydrologic modifications (e.g. construction of Keban Dam and Eyüpbağları Pumping-Irrigation Project), discharge of municipal wastewaters, overuse of fertilizers and animal feedlot operations, and intermittent use of saline surface waters (e.g. from Hazar Lake) in the past for irrigation purposes, probably have not only distorted the natural recharge-discharge equilibrium of the UBAS, but also shifted geochemical equilibrium in the aquifer system. As-contaminated water resources identified in the UBAS may have serious health implications for the people and environment, especially given that currently groundwater is heavily relied upon to fulfill agricultural irrigation and drinking-water demands, not only for the basin itself, but also for the entire Elazığ province (population 583,671). This study is expected to provide the much needed baseline data which will allow identify the areas where the main monitoring efforts that should be focused for the proper environmental management and sustainable development of soil and water resources of the Uluova basin. Results of this study suggest that As contamination is not only restricted to the western half of the Turkey and may be more prevalent throughout the country than previously thought. More hydrogeologic and geochemical surveys should be conducted (especially in the eastern half of the counrty) systematically to complete the currently incomplete *arsenic puzzle* for Turkey.

Conflicts of interest

The authors declare that there are no conflicts of interest regarding the publication of this paper.

Author contribution statement

M.Ç., and S.T., Conceptualization; Funding acquisition, Investigation; Project administration.

M.Ç., and C.G., Methodology, Software, Visualization; Data analysis; Writing – original draft.

M.Ç., C.G., and M.A.K., Analytical tools; Formal analysis; Validation; Data curation.

Acknowledgments

The work reported in this paper is based on part of the senior author's dissertation research which was funded by Çukurova University Scientific Research Projects Unit, Turkey (BAP) under the grant number MMF2013D6. We are indebted to Ertuğrul Çanakçı (Çukurova University) for AAS analyses of the stream sediment and soil samples. This manuscript in draft was presented at the 68th Geological Congress of Turkey held by Mineral Research & Exploration General Directorate (MTA), Ankara, Turkey (April 6–10, 2015). The authors would like to acknowledge the participants who made insightful comments and suggestions at the presentation.

References

Abderahman, N., Abu-Rukah, Y.H., 2006. An assessment study of heavy metal distribution within soil in upper course of Zarqa River basin/Jordan. Environ. Geol. 49 (8), 1116–1124.

Abdul, K.S.M., Jayasinghe, S.S., Chandana, E.P.S., Jayasumana, C., De Silva, P.M.C.S., 2015. Arsenic and human health effects: A review. Environ. Toxicol. Pharmacol. 40 (3), 828–846.

Adriano, D.C., 2001. Trace Elements in Terrestrial Environments: Biogeochemistry, Bioavailability, and Risks of Metals, 2nd ed. Springer, New York.

Akçay, M., Özkan, H.M., Moon, C.J., Scott, B.C., 1996. Secondary dispersion from gold deposits in west Turkey. J. Geochem. Explor. 56 (3), 197–218.

Akgül, B., 1987. Keban Yöresi Metamorfik Kayaçların Petrografik İncelenmesi. Unpublished MSc thesis, Fırat Üniversitesi Fen Bilimleri Enstitüsü, 67 p (in Turkish).

Akgül, B., 1993. Piran Köyü (Keban) Çevresindeki Magmatik Kayaçların Petrografik ve Petrolojik Özellikleri. Unpublished PhD dissertation, Fırat Üniversitesi Fen Bilimleri Enstitüsü, 125 p (in Turkish).

Akgul, M., 2016. The origin of the mineralizing fluids in different type mineralizations associated with the Upper Cretaceous Elazig Magmatic Complex, Turkey; an isotopic approach. J. Afr. Earth Sci. 116, 160–169.

Akkus, S., Bal, T., Karaaslan, N.M., Yaman, E., Kilinc, E., Yaman, M., 2013. Fractionation of Ni, Cr and Cu from soil by sequential extraction procedure and determination by Inductively Coupled Plasma Optical Emission Spectrometry. Clean Soil Air Water 41 (12), 1229–1234.

Aksoy, E., İnceöz, M., Koçyiğit, A., 2007. Lake Hazar Basin: A negative flower structure on the East Anatolian Fault System (EAFS) SE Turkey. Turk. J. Earth Sci. 16 (3), 319–338.

Aksoy, E., Türkmen, İ., Turan, M., 2005. Tectonics and sedimentation in convergent margin basins: an example from the Tertiary Elazığ basin, Eastern Turkey. J. Asian Earth Sci. 25 (3), 459–472.

Aksoy, N., Şimşek, C., Gunduz, O., 2009. Groundwater contamination mechanism in a geothermal field: A case study of Balcova, Turkey. J. Contam. Hydrol. 103 (1–2), 13–28.

Aktaş, G., Robertson, A.H.F., 1984. The Maden Complex, SE Turkey: evolution of a Neotethyan active margin. Geol. Soc. London Spec. Publ. 17, 375–402.

Aktug, B., Ozener, H., Dogru, A., Sabuncu, A., Turgut, B., Halicioglu, K., Yilmaz, O., Havazli, E., 2016. Slip rates and seismic potential on the East Anatolian Fault System using an improved GPS velocity field. J. Geodyn. 94–95, 1–12.

Alloway, B.J., 2013. In: Alloway, B.J. (Ed.), Heavy Metals in Soils, Trace Metals and Metalloids in Soils and their Bioavailability, 3rd ed. Springer, Dordrecht, pp. 11–50.

Altaş, L., Işık, M., Kavurmacı, M., 2011. Determination of arsenic levels in the water resources of Aksaray Province, Turkey. J. Environ. Manage. 92 (9), 2182–2192.

Altunbey, M., Sağıroğlu, A., 1995. Koçkale-Elazığ manganez cevherleşmelerinin özellikleri ve kökeni. MTA Derg. 117, 139–148 (in Turkish).

Amini, M., Abbaspour, K.C., Berg, M., Winkel, L., Hug, S.J., Hoehn, E., Yang, H., Johnson, C.A., 2008. Statistical modeling of global geogenic arsenic contamination in groundwater. Environ. Sci. Technol. 42 (10), 3669–3675.

APHA-AWWA-WEF, Standard Methods for the Examination of Water and Wastewater 21st ed. 2005 American Public Health Association-American Water Works Association-Water Environment Federation Washington, DC.

ATSDR, 2015. ToxFAQs™ for Arsenic: Agency for Toxic Substances and Disease Registry. http://www.atsdr.cdc.gov/toxfaqs/TF.asp?id=19&tid=3 (Accessed 14 March 2016).

B.U. KOERI-RETMC (Boğaziçi University Kandilli Observatory and Earthquake Research Institute - Regional Earthquake-Tsunami Monitoring Center), 2017. Earthquake Catalog Search System. http://www.koeri.boun.edu.tr/sismo/2/earthquake-catalog (Accessed 14 January 2018).

Baba, A., Yuce, G., Deniz, O., Ugurluoglu, D.Y., 2009. Hydrochemical and isotopic composition of Tuzla geothermal field (Canakkale-Turkey) and its environmental impacts. Environ. Forensics 10 (2), 144–161.

Benzer, S., 2017. Concentrations of arsenic and boron in water, sediment and the tissues of fish in Emet Stream (Turkey). Bull. Environ. Contam. Toxicol. 98 (6), 805–810.

Biasioli, M., Barberis, R., Ajmone-Marsan, F., 2006. The influence of a large city on some soil properties and metals content. Sci. Total Environ. 356 (1–3), 154–164.

Bölücek, C., Akgül, M., Türkmen, I., 2004. Volcanism, sedimentation and massive sulfide mineralization in a Late Cretaceous arc-related basin, Eastern Taurides, Turkey. J. Asian Earth Sci. 24, 349–360.

Box, G.E.P., Cox, D.R., 1964. An analysis of transformations. J. R Stat. Soc. Series B 26 (2), 211–252.

Bradl, H.B., 2004. Adsorption of heavy metal ions on soils and soils constituents. J. Colloid Interface Sci. 277 (1), 1–18.

Brookins, D.G., 1988. Eh-pH Diagrams for Geochemistry. Springer-Verlag, New York.

Bryant, F.B., Yarnold, P.R., 1995. Principal-components analysis and exploratory and confirmatory factor analysis. In: Grimm, L.G., Yarnold, P.R. (Eds.), Reading and Understanding Multivariate Statistics (pp. 99–136). American Psychological Association, Washington, DC, pp. 373.

Bundschuh, J., Bhattacharya, P., Nath, B., Naidu, R., Ng, J., Guilherme, L.R.G., Ma, L.Q., Kim, K.-W., Jean, J.-S., 2013. Arsenic ecotoxicology: The interface between geosphere, hydrosphere and biosphere. J. Hazard. Mater. 262, 883–886.

Calayır, Y., Sayın, E., Yön, B., 2012. Performance of structures in the rural area during the March 8, 2010 Elazığ-Kovancılar earthquake. Nat. Hazards 61, 703–717.
Candeias, C., Melo, R., Ávila, P.F., da Silva, E.F., Salgueiro, A.R., Teixeira, J.P., 2014. Heavy metal pollution in mine–soil–plant system in S. Francisco de Assis – Panasqueira mine (Portugal). Appl. Geochem. 44, 12–26.
Caritat, P., Reimann, C., 2012. NGSA Project Team GEMAS Project Team Comparing results from two continental geochemical surveys to world soil composition and deriving Predicted Empirical Global Soil (PEGS2) reference values. Earth Planet. Sci. Lett. 319–320, 269–276.
Çeliker, M., 2008. Uluova'nın (Elazığ) Hidrojeolojisinin Coğrafi Bilgi Sistemleri ile İncelenmesi. Çukurova Üniversitesi Fen Bilimleri Enstitüsü, Unpublished MSc thesis, 118 p (in Turkish).
Çeliker, M., 2014. Elazığ Uluova Yeraltısuyu Akiferinin Arsenik ve Ağır Metal İçeriğinin Araştırılması. Çukurova Üniversitesi Fen Bilimleri Enstitüsü, Unpublished PhD dissertation, 254 p (in Turkish).
Çeliker, M., 2016. Determination of the interaction between groundwater and surface water using environmental isotopes (Oxygen-18, Deuterium and Tritium) and chemical analyses in Uluova Region, Elazig, Turkey. J. Eng. Res. 4 (1), 105–124.
Çetindağ, B., 1985. Elazığ, Palu-Kovancılar Dolayının Hidrojeoloji İncelemesi. Fırat Üniversitesi Fen Bilimleri Enstitüsü, Unpublished MSc thesis, 133 p (in Turkish).
Çetindağ, B., Okan, Ö.Ö., 2004. Hydrochemical characteristics and pollution potential of Uluova aquifers, Elazığ, Turkey. Environ. Geol. 45 (6), 796–807.
Çolak, M., Gemici, Ü., Tarcan, G., 2003. The effects of colemanite deposits on the arsenic concentrations of soil and ground water in Igdeköy-Emet, Kütahya, Turkey. Water Air Soil Pollut. 149 (1), 127–143.
Çolak, S., Aksoy, E., Koçyiğit, A., İnceöz, M., 2012. The Palu-Uluova strike-slip basin in the East Anatolian Fault System, Turkey: Its transition from the Palaeotectonic to Neotectonic stage. Turk. J. Earth Sci. 21, 547–570.
Davidson, C.M., 2013. Methods for the determination of heavy metals and metalloids in soils. In: Alloway, B.J. (Ed.), Heavy Metals in Soils, Trace Metals and Metalloids in Soils and their Bioavailability, 3rd ed. Springer, Dordrecht, pp. 97–140.
Davis, J.C., 2002. Statistics and Data Analysis in Geology, 3rd ed. John Wiley & Sons Inc, New York.
Domenico, P.A., Schwartz, F.W., 1997. Physical and Chemical Hydrogeology, 2nd ed. John Wiley & Sons Inc., New York.
DSİ (General Directorate of State Hydraulic Works), 2012. Elazığ–Uluova Projesi Uluova Sulaması Planlama Revize Arazi Sınıflandırma ve Drenaj Raporu, DSİ IX. Bölge Müdürlüğü, Elazığ (in Turkish).
DSİ (General Directorate of State Hydraulic Works), 2015. Gözlem İstasyonları Yönetim Sistemi. http://rasatlar.dsi.gov.tr/# (Accessed 22 February 2018).
EEC, 1998. Council Directive 98/83/EC of 3 November 1998 on the quality of water intended for human consumption. Official Journal L 330/32, 05.12.1998. http://eur-lex.europa.eu/legal-content/EN/TXT/PDF/?uri=CELEX:31998L0083&from=EN (Accessed 20 January 2017).
Eliopoulos, D.G., Economou-Eliopoulos, M., Apostolikas, A., Golightly, J.P., 2012. Geochemical features of nickel-laterite deposits from the Balkan Peninsula and Gordes, Turkey: The genetic and environmental significance of arsenic. Ore Geol. Rev. 48, 413–427.
ESRI (Environmental Systems Research Institute), 2009. ArcMap 9.3.1. 380 New York Street, Redlands, CA 92373-8100, USA.
Facchinelli, A., Sacchi, E., Mallen, L., 2001. Multivariate statistical and GIS-based approach to identify heavy metal sources in soils. Environ. Pollut. 114, 313–324.
García-Veigas, J., Rosell, L., Ortí, F., Gündoğan, İ., Helvacı, C., 2011. Mineralogy, diagenesis and hydrochemical evolution in a probertite–glauberite–halite saline lake (Miocene, Emet Basin, Turkey). Chem. Geol. 280, 352–364.
Gemici, Ü., Tarcan, G., 2004. Hydrogeological and hydrogeochemical features of the Heybeli Spa, Afyon, Turkey: Arsenic and the other contaminants in the thermal waters. Bull. Environ. Contam. Toxicol. 72 (6), 1107–1114.
Gemici, Ü., Tarcan, G., Somay, A.M., Akar, T., 2009. Factors controlling the element distribution in farming soils and water around the abandoned Halıköy mercury mine (Beydağ, Turkey). Appl. Geochem. 24, 1908–1917.
Gjoka, F., Felix-Henningsen, P., Wegener, H.-R., Salillari, I., Beqiraj, A., 2011. Heavy metals in soils from Tirana (Albania). Environ. Monit. Assess. 172 (1), 517–527.
Glendell, M., Granger, S.J., Bol, R., Brazier, R.E., 2014. Quantifying the spatial variability of soil physical and chemical properties in relation to mitigation of diffuse water pollution. Geoderma 214–215, 25–41.
Goldberg, S., Hyun, S., Lee, L.S., 2008. Chemical modeling of arsenic(III, V) and selenium (IV, VI) adsorption by soils surrounding ash disposal facilities. Vadose Zone J. 7, 1185–1192.
Güler, C., Alpaslan, M., Kurt, M.A., Temel, A., 2010. Deciphering factors controlling trace element distribution in the soils of Karaduvar industrial-agricultural area (Mersin, SE Turkey). Environ. Earth Sci. 60 (1), 203–218.
Güler, C., Kurt, M.A., Alpaslan, M., Akbulut, C., 2012. Assessment of the impact of anthropogenic activities on the groundwater hydrology and chemistry in Tarsus coastal plain (Mersin, SE Turkey) using fuzzy clustering, multivariate statistics and GIS techniques. J. Hydrol. 414–415, 435–451.
Güler, C., Thyne, G.D., 2004. Hydrologic and geologic factors controlling surface and groundwater chemistry in Indian Wells-Owens Valley area, southeastern California. USA. J. Hydrol. 285 (1–4), 177–198.
Güler, C., Thyne, G.D., McCray, J.E., Turner, A.K., 2002. Evaluation of graphical and multivariate statistical methods for classification of water chemistry data. Hydrogeol. J. 10 (1), 455–474.
Güler, C., Thyne, G.D., Tağa, H., Yıldırım, Ü., 2017. Processes governing alkaline groundwater chemistry within a fractured rock (ophiolitic mélange) aquifer underlying a seasonally inhabited headwater area in the Aladağlar Range (Adana, Turkey). Geofluids 1–21. https://doi.org/10.1155/2017/3153924. Article ID 3153924.
Gunduz, O., Simsek, C., Hasozbek, A., 2010. Arsenic pollution in the groundwater of Simav plain, Turkey: Its impact on water quality and human health. Water Air Soil Pollut. 205, 43–62.
Hem, J.D., 1985. Study and Interpretation of the Chemical Characteristics of Natural Water, 3rd edition. United States Geological Survey Water-Supply Paper 2254, Washington DC, USA.
Jaffey, N., Robertson, A., 2005. Non-marine sedimentation associated with Oligocene-Recent exhumation and uplift of the Central Taurus Mountains, S Turkey. Sediment. Geol. 173 (1–4), 53–89.
Johnson, J.E., Anderson, G., Parkhurst, D., 2000. "thermo.com.V8.R6.230", Version 1.11. Lawrence Livermore National Laboratory.
Kabata-Pendias, A., Pendias, H., 2001. Trace Elements in Soils and Plants, 3rd ed. CRC Press, Boca Raton, Florida.
Kaiser, H.F., 1960. The application of electronic computers to factor analysis. Educ. Psychol. Meas. 20, 141–151.
Kalender, L., Uçar, S.Ç., 2013. Assessment of metal contamination in sediments in the tributaries of the Euphrates River, using pollution indices and the determination of the pollution source, Turkey. J. Geochem. Explor. 134, 73–84.
Karanjac, J., Altunkaynak, M., Övül, G., 1977. Mathematical model of Uluova Plain, Turkey – A training and management tool. Ground Water 15 (5), 348–357.
Karayigit, A.I., Spears, D.A., Booth, C.A., 2000. Antimony and arsenic anomalies in the coal seams from the Gokler coalfield, Gediz, Turkey. Int. J. Coal Geol. 44 (1), 1–17.
Kaya, A., 2004. Gezin (Maden-Elazığ) çevresinin jeolojisi. Pamukkale Üniv. Mühendis. Fak. Mühendis. Bilim. Derg., pp. 41–50 (in Turkish).
Kerey, E., Türkmen, İ., 1991. Palu Formasyonu'nun (Pliyosen-Kuvaterner) sedimantolojik özellikleri, Elazığ doğusu. Turk. Jeol. Bul. 34, 21–26 (in Turkish).
Kolmogorov, A.N., 1933. Sulla determinazione empirica di una legge di distribuzione. Giornale dell'Istituto Italiano degli Attuari 4, 83–91 (in Italian).
Korte, M.E., Fernando, Q., 1991. A review of arsenic (III) in groundwater. Crit. Rev. Environ. Contr. 21, 1–39.
Lawrence, F.W., Upchurch, S.B., 1982. Identification of recharge areas using geochemical factor analysis. Groundwater 20 (6), 680–687.
Lindsay, W.L., 1979. Chemical Equilibria in Soils. John Wiley & Sons Ltd., Chichester, Sussex.
Machiwal, D., Cloutier, V., Güler, C., Kazakis, N., 2018. A review of GIS-integrated statistical techniques for groundwater quality evaluation and protection. Environ. Earth Sci. 77, 681. https://doi.org/10.1007/s12665-018-7872-x.
Mandal, B.K., Suzuki, K.T., 2002. Arsenic round the world: a review. Talanta 58, 201–235.
May, T.W., Wiedmeyer, R.H., 1998. A table of polyatomic interferences in ICP-MS. At. Spectrosc. 19 (5), 150–155.
Ministry of Environment and Forestry, 2014. Elazığ İli 2014 Yılı Çevre Durum Raporu. http://www.csb.gov.tr/db/ced/editordosya/Elazig%202014.pdf (Accessed 25 March 2016).
Mukherjee, A., Verma, S., Gupta, S., Henke, K.R., Bhattacharya, P., 2014. Influence of tectonics, sedimentation and aqueous flow cycles on the origin of global groundwater arsenic: Paradigms from three continents. J. Hydrol. 518, 284–299.
National Research Council, 1977. Arsenic: Medical and Biologic Effects of Environmental Pollutants. National Academy of Sciences, Washington, DC.
Nordberg, G., 1998. Metals: chemical properties and toxicity. In: Stellman, J.M. (Ed.), Encyclopedia of Occupational Health and Safety, 4th ed. International Labour Organization, Geneva.
Nordstrom, D.K., 2000. An overview of arsenic mass poisoning in Bangladesh and West Bengal, India. In: Young, C. (Ed.), Minor Elements 2000: Processing and Environmental Aspects of As, Sb, Se, Te, and Bi. Society for Mining, Metallurgy and Exploration, pp. 21–30.
Olgun, K., Kalkan, S., 1994. Elazığ-Uluova Revize Etüt Raporu. Devlet Su İşleri, Ankara (in Turkish).
Özgül, N., 1984. Stratigraphy and tectonic evolution of the Central Taurides. In: Tekeli, O., Göncüoğlu, M.C. (Eds.), International Symposium on the Geology of the Taurus Belt. Maden Tetkik ve Arama Enstitüsü, Ankara, pp. 77–90.
Özkul, C., Çiftçi, E., Köprübaşı, N., Tokel, S., Savaş, M., 2015. Geogenic arsenic anomalies in soils and stream waters of Neogene Emet basin (Kütahya-Western Turkey). Environ. Earth Sci. 73 (10), 6117–6130.
Öztekin, Ö., 1998. Elazığ İli İçme ve Kullanma Sularının Fiziko-Kimyasal Özellikleri. Fırat Üniversitesi Fen Bilimleri Enstitüsü, Unpublished MSc thesis, 124 p (in Turkish).
Palutoğlu, M., Tanyolu, E., 2006. Elazığ il merkezi yerleşim alanının depremselliği. Fırat Üniv. Fen Mühendis. Bilim. Derg. 18 (4), 577–588 (in Turkish).
Parkhurst, D.L., Appelo, C.A.J., 2015. Description of input and examples for PHREEQC version 3 − A computer program for speciation, batch-reaction, one-dimensional transport, and inverse geochemical calculations, U.S. Geological Survey Techniques and Methods, book 6, chap. A43. http://pubs.usgs.gov/tm/06/a43/ (Accessed 10 June 2016).
Pasvanoğlu, S., 2013. Hydrogeochemistry of thermal and mineralized waters in the Diyadin (Ağri) area, Eastern Turkey. Appl. Geochem. 38, 70–81.
Pasvanoğlu, S., Chandrasekharam, D., 2011. Hydrogeochemical and isotopic study of thermal and mineralized waters from the Nevşehir (Kozakli) area Central Turkey. J. Volcanol. Geotherm. Res. 202 (3–4), 241–250.
Perinçek, D., 1979. The geology of Hazro-Korudağ-Çüngüş-Maden-Ergani-Hazar-Elazığ-Malatya area. Guide Book, Geological Society of Turkey, pp. 33.
Peters, S.C., Blum, J.D., Klaue, B., Karagas, M.R., 1999. Arsenic occurrence in New Hampshire drinking water. Environ. Sci. Technol. 33, 1328–1333.
Piper, A.M., 1944. A graphic procedure in the geochemical interpretation of water-analyses. Trans Am. Geophys. Union 25, 914–923.
Plant, J.A., Kinniburgh, D.G., Smedley, P.L., Fordyce, F.M., Klinck, B.A., 2003. Arsenic and selenium, Treatise on Geochemistry, Chapter 9.02. Elsevier Ltd., Amsterdam, pp.

17–66.
Querol, X., Whateley, M.K.G., Fernández-Turiel, J.L., Tuncali, E., 1997. Geological controls on the mineralogy and geochemistry of the Beypazari lignite, central Anatolia, Turkey. Intern. J. Coal Geol. 33 (3), 255–271.
Core Team, R., 2014. R: A language and environment for statistical computing. R Foundation for Statistical Computing, Vienna http://www.R-project.org/.
Rahman, M., 2002. Arsenic and contamination of drinking-water in Bangladesh: A public-health perspective. J. Health, Popul. Nutr. 20 (3), 193–197.
Ratnaike, R.N., 2003. Acute and chronic arsenic toxicity. Postgrad. Med. J. 79, 391–396.
Ravenscroft, P., Brammer, H., Richards, K., 2009. Arsenic pollution: a global synthesis. RGS-IBG Book Series. Wiley-Blackwell, Oxford.
Raychowdhury, N., Mukherjee, A., Bhattacharya, P., Johannesson, K., Bundschuh, J., Sifuentes, G.B., Nordberg, E., Martin, R.A., Storniolo, A.R., 2014. Provenance and fate of arsenic and other solutes in the Chaco-Pampean Plain of the Andean foreland, Argentina: From perspectives of hydrogeochemical modeling and regional tectonic setting. J. Hydrol. 518, 300–316.
Rudnick, R.L., Gao, S., 2014. Composition of the Continental Crust, pp. 1–51. In: The Crust (ed. Rudnick, R.L.), vol. 4, Treatise On Geochemistry (eds. Holland, H.D. and Turekian, K.K.), 2nd ed., Elsevier-Pergamon, Oxford.
Sagiroglu, A., Sasmaz, A., 2004. Mineralogy and geochemistry of the argentiferous Pb–Zn and Cu veins of the Çolaklı area, Elazig, Eastern Turkey. J. Asian Earth Sci. 23, 37–45.
Santi, P.M., McCray, J.E., Martens, J.L., 2006. Investigating cross-contamination of aquifers. Hydrogeol. J. 14, 51–68.
Şaşmaz, A., Türkyilmaz, B., Öztürk, N., Yavuz, F., Kumral, M., 2014. Geology and geochemistry of Middle Eocene Maden complex ferromanganese deposits from the Elazığ-Malatya region, eastern Turkey. Ore Geol. Rev. 56, 352–372.
Scanlon, B.R., Nicot, J.P., Reedy, R.C., Kurtzman, D., Mukherjee, A., Nordstrom, D.K., 2009. Elevated naturally occurring arsenic in a semiarid oxidizing system, Southern High Plains aquifer, Texas, USA. Appl. Geochem. 24, 2061–2071.
Selene, C.-H., Chou, J., De Rosa, C.T., 2003. Case studies – Arsenic. Intern. J. Hyg. Environ. Health 206 (4–5), 381–386.
Simsek, C., 2013. Assessment of naturally occurring arsenic contamination in the groundwater of Sarkisla Plain (Sivas/Turkey). Environ. Earth Sci. 68 (3), 691–702.
Smedley, P.L., Kinniburgh, D.G., 2002. A review of the source, behaviour and distribution of arsenic in natural waters. Appl. Geochem. 17 (5), 517–568.
Smirnov, N., 1948. Table for estimating the goodness of fit of empirical distributions. Ann. Math. Stat. 19 (2), 279–281.
Sungurlu, O., Perinçek, D., Kurt, G., Tuna, E., Dülger, S., Çelikdemir, E., Naz, H., 1985. Geology of the Elazığ-Hazar-Palu area. Türk Cumhur. Pet. İşleri Genel Müdür. Derg. 29, 83–191.
Turkish State Meteorological Service, 2016. http://www.mgm.gov.tr/veridegerlendirme/il-ve-ilceler-istatistik.aspx?m=ELAZIG#sfB (Accessed 25 February 2016).
Turkish Statistical Institute, 2018. http://www.tuik.gov.tr/PreIstatistikTablo.do?istab_id=1590 (Accessed 25 March 2018).
USDA, 1999. Soil Taxonomy. A Basic System of Soil Classification for Making and Interpreting Soil Surveys, Handbook No. 436. Soil Survey Staff, Washington, DC.
USEPA, 2009. National Primary Drinking Water Regulations. https://www.epa.gov/ground-water-and-drinking-water/table-regulated-drinking-water-contaminants#Inorganic (Accessed 20 January 2017).
WHO (World Health Organization), 1993. Guidelines for drinking-water quality, 2nd edition. Vol. 1 – Recommendations: Chemical aspects. http://www.who.int/water_sanitation_health/dwq/2edvol1c.pdf (Accessed 14 March 2016).
WHO (World Health Organization), 2011. Guidelines for Drinking-water Quality, 4th ed., WHO, Geneva. Available online: http://whqlibdoc.who.int/publications/2011/9789241548151_eng.pdf (Accessed 15 January 2017).
Woolson, E.A., 1983. Emissions, cycling and effects of arsenic in soil ecosystems. In: Fowler, B.A. (Ed.), Biological and Environmental Effects of Arsenic. Topics in Environmental Health. Elsevier, New York.
Yılmaz, H., 2007. Stream sediment geochemical exploration for gold in the Kazdağ dome in the Biga peninsula, western Turkey. Turk. J. Earth Sci. 16 (1), 33–55.
Yılmaz, Y., Yiğitbaş, E., Genç, S.C., 1993. Ophiolitic and metamorphic assemblages of southeast Anatolia and their significance in the geological evolution of the orogenic belt. Tectonics 12 (5), 1280–1297.
Yuce, G., Yasin, D.U., 2012. Assessment of an increase in boron and arsenic concentrations at the discharge area of Na-borate mine (Kirka-Eskisehir, Turkey). Terr. Atmos. Ocean. Sci. 23 (6), 703–723.
Zhou, Q., Teng, Y., Liu, Y., 2017. A study on soil-environmental quality criteria and standards of arsenic. Appl. Geochem. 77, 158–166.